AD-A146 156 THE DETERMINATION OF THE SMOKE HAZARDS RESULTING FROM THE BURNING OF SHIPBOARD MATERIALS UTILIZED BY THE US NAVY(U) GEORGIA INST OF TECH ATLANTA 31 AUG 81 1/1

UNCLASSIFIED N00014-78-C-0771 F/G 13/12 NL

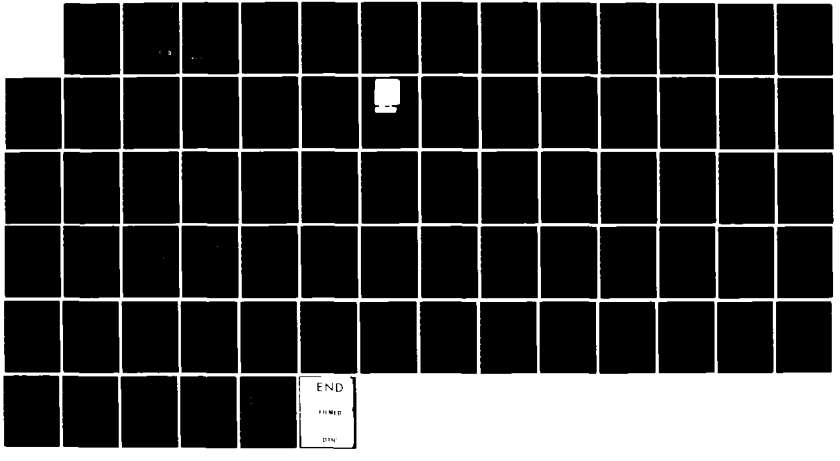

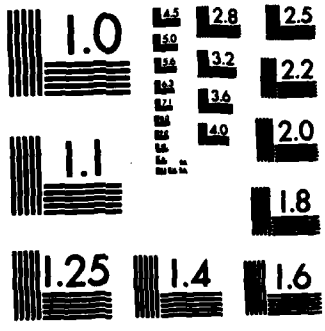

MICROCOPY RESOLUTION TEST CHART

Georgia Institute of Technology, Atlanta, GA
School of Aerospace Engineering
Contract No. N00014-78-C-0771
N00014-80-C-0432

Title: Determination of the Smoke Hazards Resulting From the Burning of Shipboard Materials Utilized by the US Navy

Period Covered: 1 Sept. 1980-31 Aug. 1981
Date of Report: 31 Aug. 1981

CONTENTS

ABSTRACT

Further investigations have been conducted to evaluate the hazards due to smoke formation in shipboard fires. The physical and chemical properties of the smoke particulates generated during combustion were determined for a polyphosphazene foam which is being considered by the Navy for use as a thermal and acoustic insulation material in submarines. Physical properties measured were particle size distribution and mean particle diameter, mass fraction of fuel converted to particulates, optical density, particle refractive index, and particulate volume fraction. The dependence of these properties on the temperature of the test-chamber atmosphere and the mode of combustion (flaming or smoldering) was determined. Chemical analysis of the smoke particulates determined the major toxic species generated by the combustion of this material.

Results of this study indicate that during nonflaming combustion, this polyphosphazene foam produces smoke particles with a log-normal size distribution and a mean diameter of about 0.45 micron. During flaming combustion the polyphosphazene produced black smoke consisting of nonspherical soot aggregates with a mean particle diameter (D_{32}) between 0.9 and 1.2 microns. The greatest light obscuration was obtained under nonflaming combustion at a radiant flux of 7.5 W/cm^2. For nonflaming combustion, moderate increases in ambient temperature result in decreases in peak volume fraction and total particle volume, while above 300°C no particles are produced. For flaming combustion, moderate ambient temperature increases have little effect on peak optical density and peak volume fraction, while total particulate volume is decreased. Above 300°C the period of strong flaming combustion is much longer resulting in much larger values of peak optical density, peak volume fraction and total particulate volume. Also mean particle diameter increases with ambient temperature for flaming combustion. These results indicate that the loss of visibility due to smoke formation during combustion of the polyphosphazene foam in shipboard fires is considerably less than that obtained with the previously tested PVC-nitrile rubber insulation.

Chemical analysis of the smoke particulates generated during nonflaming combustion indicated the presence of aliphatic hydrocarbons, oxygenated aliphatic hydrocarbons, aliphatic nitriles, polynuclear aromatic hydrocarbons and oxygenated aromatic compounds, while organophosphorus compounds were not detected. The level of hydrogen cyanide expected from thermal decomposition of the aliphatic nitrile species is well below the amount likely to produce acute toxic hazard to personnel exposed to gases in a fire.

INTRODUCTION

This report describes the efforts conducted for the Naval Research Laboratory under Contract No. N00014-78-C-0771 entitled "The Determination of the Smoke Hazards Resulting from the Burning of Shipboard Materials Utilized by the U.S. Navy." This work, which was performed during the period September 1, 1980 through August 31, 1981, was concerned with the evaluation of the hazards due to smoke formation in shipboard fires. Specifically, this research program is a continuation of work done during the previous two years to determine the physical and chemical properties of smoke particulates generated during the combustion of representatives of three classes of materials abundantly present on shipboard. In the present investigation, the same measurements were obtained for a polyphosphazene foam, which is being considered by the Navy as a thermal and acoustic insulation material for use in submarines. The aims of this investigation were: (1) the identification of conditions under which large quantities of smoke that would result in severe light obscuration are generated; (2) the identification of major toxic species which are associated with the smoke particulates generated during the combustion of the polyphosphazene material; and (3) the identification of compounds present in the smoke particulates which are possible precursors to smoke formation.

To pursue the objectives outlined above, the efforts of this research project have been divided into two major tasks. Task A is concerned with the measurements of the physical properties of the smoke particulates, while Task B deals with the chemical analysis of the combustion products.

This program has been directed by Dr. Ben T. Zinn in the School of Aerospace Engineering of the Georgia Institute of Technology. He was assisted by Dr. R. F. Browner in the School of Chemistry who was responsible for the chemical analysis work under Task B. Other senior staff members participating in the research were Drs. E. A. Powell and M. Pasternak.

EXPERIMENTAL ~~FACILITIES~~

The smoke ~~research program~~ described herein has been conducted utilizing the following facilities which have been developed at the School of Aerospace Engineering, Georgia Institute of Technology: (1) a Combustion Products Test Chamber, (2) a Combustion Products Sampling System; (3) an In Situ Optical Aerosol Measurement System; and (4) a Chemical Analysis Laboratory.

The ventilated Combustion Products Test Chamber (CPTC) shown in Figure 1 is capable of simulating a wide variety of environmental conditions that may be encountered in actual fire situations. Specifically, the design of the CPTC permits easy control and measurement of the following variables during the combustion of small samples of materials: (1) the mode of combustion (i.e., flaming vs. smoldering combustion); (2) the sample radiant heating rate (up to 10 watts/cm^2); (3) the sample weight loss during the test; (4) the composition of the ventilating gas surrounding the sample; (5) the temperature of the ventilation gas (up to 650^{o}C) and; (6) an option to test the sample under either vertical or horizontal mounting. A complete description of the CPTC including operating procedures, can be found in References 1 and 2.

During testing, a Combustion Products Sampling System shown in Figure 2 is used to analyze smoke samples that are continuously withdrawn from the gases flowing from the CPTC. Information obtained by the Aerosol Sampling System includes particle size distributions and total particulate mass generated. Some of the collected smoke samples are also retained for chemical analysis. A description of the sampling system can also be found in References 1 and 2.

In addition to the data obtained by sampling techniques, an In Situ Optical Aerosol Measurement System is utilized to make simultaneous mean particle size and concentration measurements (Figure 3). With this optical smoke analysis system measurement of scattered blue-green laser light (λ = 0.488 μm) at forward angles of 5^o and 15^o provide time-resolved data

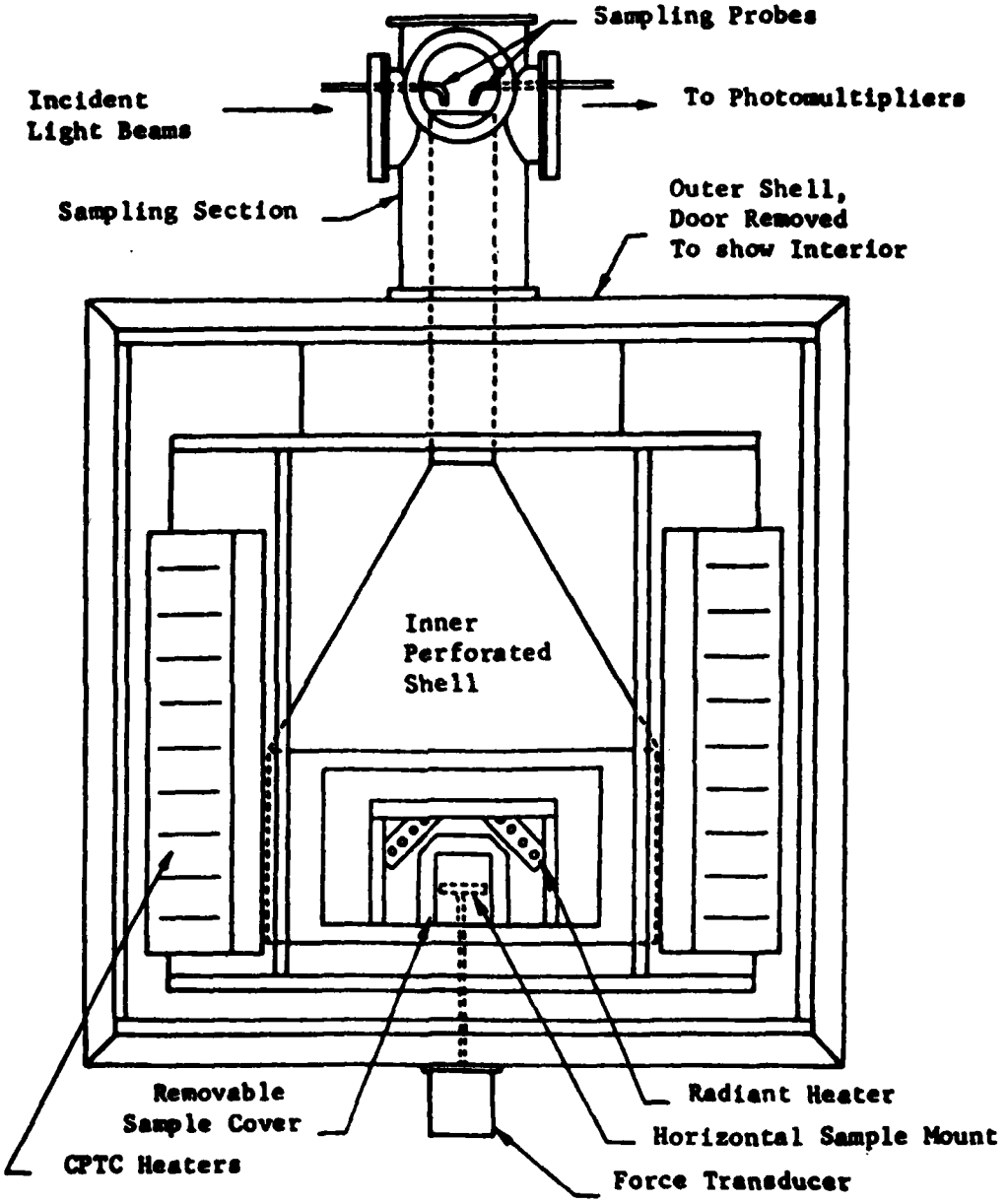

Figure 1. Combustion Products Test Chamber.

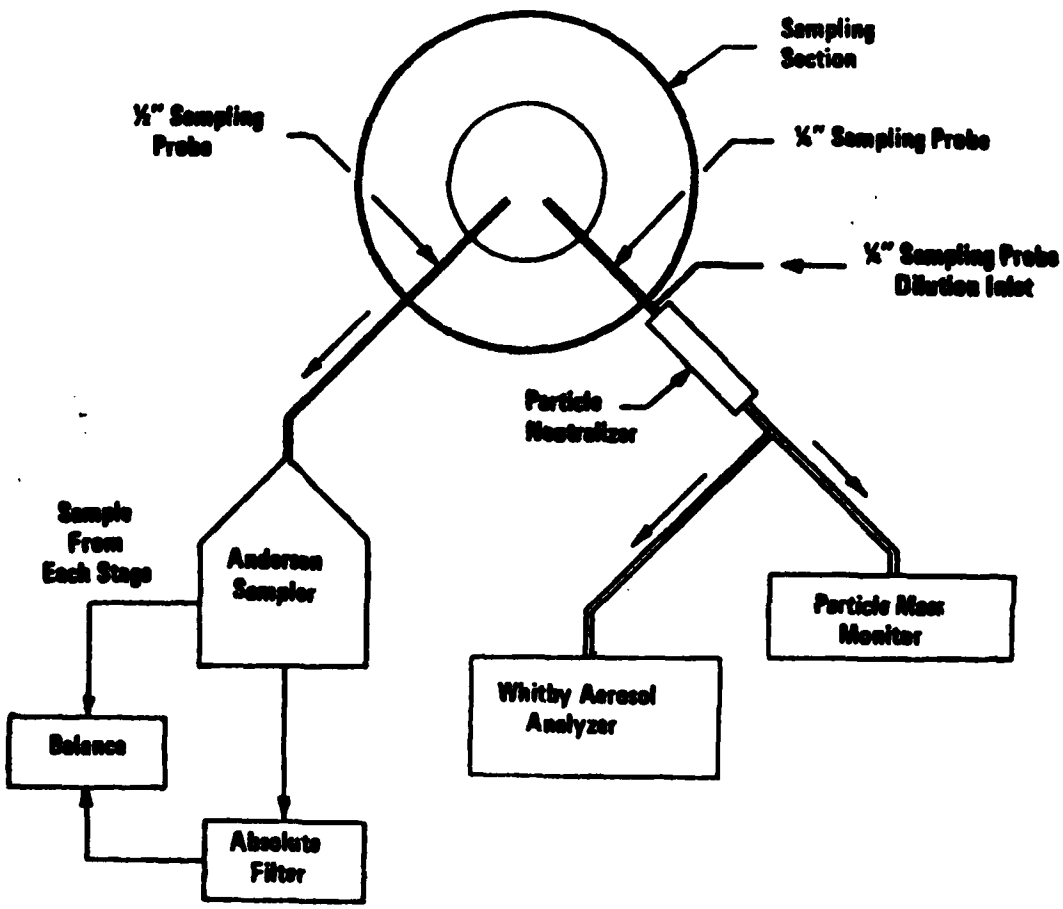

Figure 2. Combustion Products Sampling System.

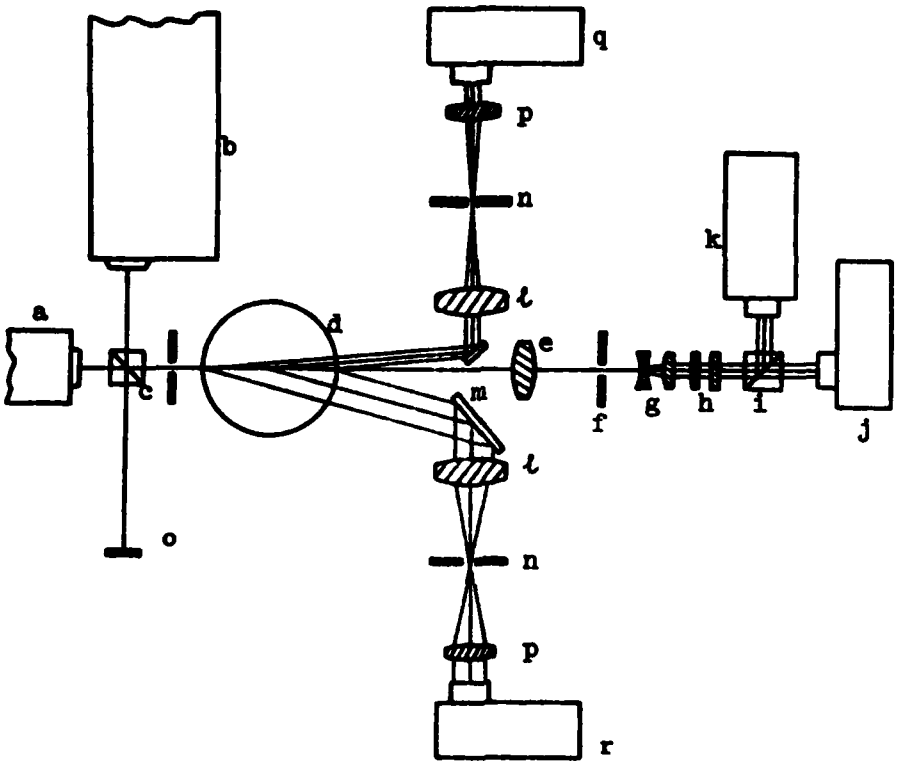

Figure 3. In situ optical aerosol measurement system:
(a) helium-neon laser, 5 mW
(b) argon-ion laser, 30 mW
(c) beam-combining cube,
(d) 11.4-cm-diam stack from the combustion products test chamber,
(e) objective lens,
(f) pinhole aperture,
(g) beam expander,
(h) neutral density filters,
(i) beam-splitter cube,
(j) transmitted blue-light detector,
(k) transmitted red-light detector,
(l) objective lenses,
(m) mirrors,
(n) pinhole apertures,
(o) light stop,
(p) collimating lenses,
(q) 5^{o}-scattering detector, and
(r) 15^{o}-scattering detector.

describing the average size of the smoke particles. Measurement of transmitted red (λ = 0.633 μm) and blue-green laser lights provide the optical densities of the smoke at these two wavelengths. For nonabsorbing particles (usually produced by nonflaming combustion) the transmitted light measurements along with the mean particle size measurements also yield the refractive index and volume concentration of the smoke particles. For absorbing particles (i.e., soot) measurements of 90°-scattered blue-green light intensities parallel to and perpendicular to the plane of polarization of the incident light beam (Figure 4) provide additional data necessary to determine the complex refractive index of the smoke particles. Details of the optical system are available in References 2,3 and 4.

An on-line data acquisition system utilizing a Hewlett-Packard 2100 mini-computer is being used for acquiring, reducing and plotting all of the optical data with the exception of the 90°-scattering data which must be reduced using the CDC Cyber 730 computer at Georgia Tech's computer center.

Finally, a chemical laboratory containing analytical equipment for the determination of the chemical composition of smoke particulates sampled during tests in the CPTC has been developed. The available equipment includes a high pressure liquid chromatograph, an infrared spectrophotometer, a gas chromatograph equipped with a thermal conductivity detector and a gas chromatograph which is equipped with dual flame ionization detectors and is interfaced to a mass spectrometer. The gas chromatograph/mass spectrometer system is also equipped with a computerized data acquisition and analysis system that records the total-ion chromatograms and the mass spectra. A digital plotter is available for obtaining high quality reproductions of the recorded data. Identification of the individual mass spectra is accomplished with the aid of the Aldermaston Spectral Library. Also, a recent addition to the chemical laboratory is a small combustion chamber and sampling system. This facility has been assembled for the accurate analysis of toxic gases absorbed on smoke particulates in conjunction with the above-described chemical analysis instrumentation.

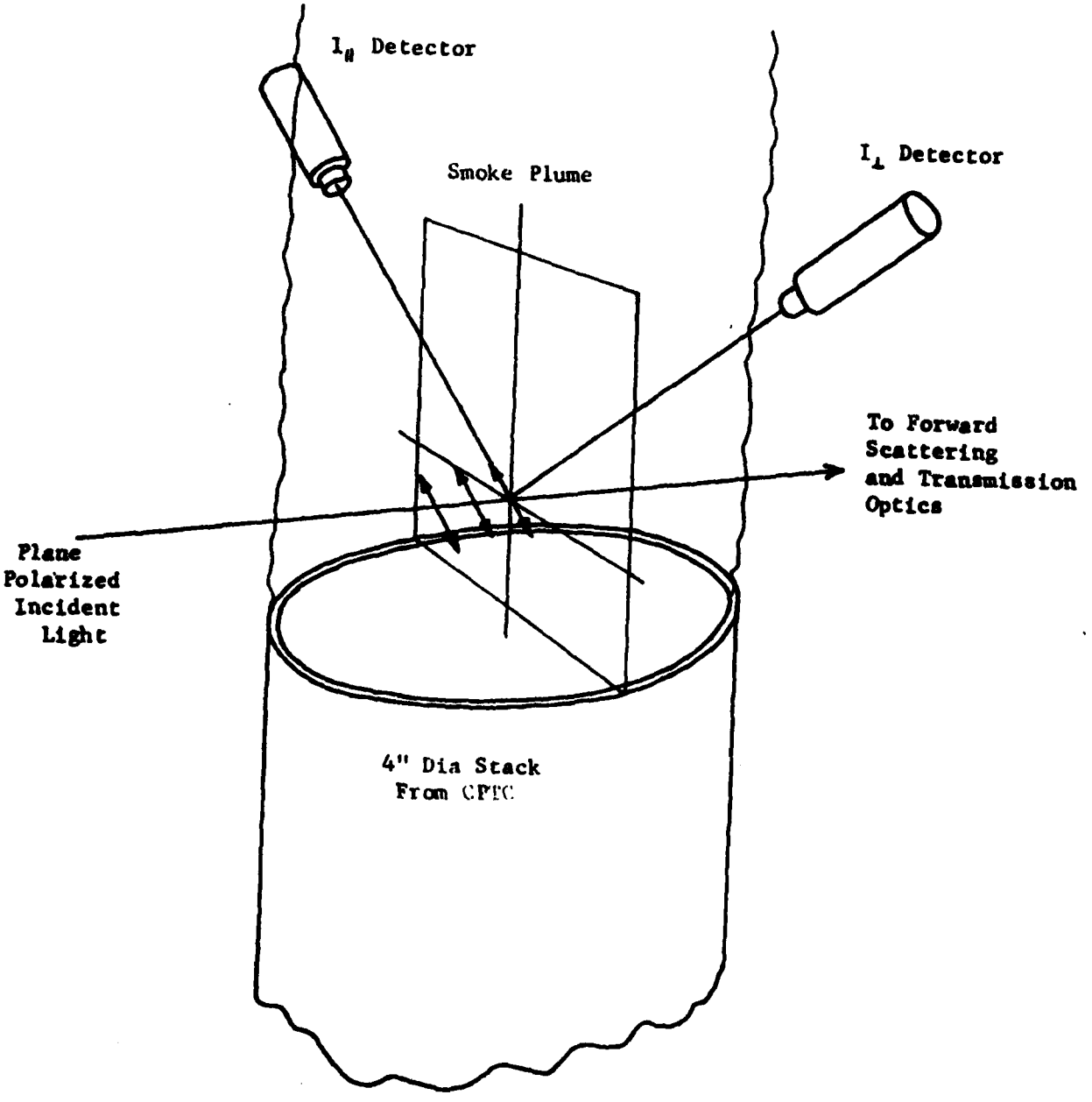

Figure 4. Optical system for 90°- scattering measurements.

TEST PROCEDURES AND CONDITIONS FOR SMOKE PHYSICAL PROPERTIES MEASUREMENTS.

A phase
~~Task A~~ of this research program was concerned with the determination of the detailed physical properties of smoke particulates generated by burning a polyphosphazene wall insulation material, which is being considered by the U. S. Navy for use aboard submarines. The material to be tested was provided by the Navy. The tests were performed by utilizing the Combustion Products Test Chamber (CPTC), the Aerosol Sampling System and the In Situ Aerosol Measurement System.

For tests conducted in room temperature ventilation gas, the physical analysis of the smoke particulates determined the following smoke properties: (1) the particle size distribution, (2) the mass fraction of fuel converted to particulates, (3) the evolution of the mean particle diameter with time, (4) the light obscuration by the particles (i.e., optical density), (5) the particle refractive index, and (6) the volume fraction (i.e., volume concentration) of the particles. For the tests conducted in hot ventilation gas, items (1) and (2) above were not determined since the Aerosol Sampling System can not be operated at high temperature. In addition the sample mass loss as a function of time was determined for most of the tests.

The dependence of the above quantities upon the following experimental conditions was determined: (1) the temperature of the test chamber atmosphere, and (2) the mode of combustion (i.e., flaming or smoldering combustion). Thus the polyphosphazene material was subjected to the test matrix shown in Table 1. All of the tests were conducted in the horizontal sample orientation, and in most of the tests the sample was exposed to a radiant heat flux of 5 W/cm^2. The determination of particulate size distributions using cascade impactor sampling was attempted for all room temperature tests. For both flaming and nonflaming tests with a radiant flux of 5 W/cm^2, the amounts of sample collected on the cascade impactor plates was insufficient for determination of the size distribution. For this reason an additional nonflaming test at 7.5 W/cm^2 was conducted

Table 1. Polyphosphazene Test Matrix.

Test	Radiant Flux (W/cm^2)	Ventilation Gas Temperature (^oC)	Type of Combustion	Ventilation Gas Composition	Flow Rate of Heated Ventilation Gas (ℓ /min)
1	5	25	Nonflaming	Air	142
2	5	100	"	"	178
3	5	300	"	"	273
4	7.5	25	"	"	142
5	5	25	Flaming	"	142
6	5	100	"	"	178
7	5	300	"	"	273

for which sufficient particulates were collected for measurement of the size distribution. In the flaming tests, the pyrolysis products generated by exposure of the sample to the 5 W/cm^2 radiant flux were ignited by a small propane pilot flame. Finally, in all tests the CPTC ventilation gas consisted of air flowing at a volumetric rate (before heating) of 142 liters per minute. Due to the decrease in density of the ventilation air during heating, the volumetric flow rate of the heated air during the high temperature tests was higher as shown in Table 1.

In the following section of this report smoke particulate physical properties data will be presented for the polyphosphazene material tested during this research program. A brief discussion of each of the measured parameters is given in Appendix A.

This material was manufactured by Horizons, Inc. Cleveland, Ohio. FWL

SMOKE PHYSICAL PROPERTIES DATA FOR POLYPHOSPHAZENE FOAM INSULATION

Description of Material.

The polyphosphazene wall insulation material tested ~~under Task A~~ was a light tan or beige colored, flexible foam material with a density of about 0.15 g/cm^3. This material was received from the Navy in the form of 36 cm x 53 cm rectangular sheets about 12 mm thick. Initially the material was cut into 7.6 cm squares with an average weight of 10 g, which completely filled the sample holder. During preliminary tests, lateral expansion of the material against the sides of the sample holder caused the sample to bulge up and contact the quartz tubes of the radiant heater. To alleviate this problem, all subsequent tests were conducted using 5.1 cm squares (2 in.) with an average weight of 4.6 g. This allowed adequate room for lateral expansion of the samples during combustion with only moderate vertical bulging.

Tests in Room Temperature Ventilation Air

Both flaming and nonflaming tests of the polyphosphazene foam insulation material were conducted under a radiant exposure of 5 W/cm^2 in room-temperature ventilation air (25^{o}C) at a flow rate of 142 l/min (5 CFM). An additional nonflaming test was conducted at a higher radiant flux of 7.5 W/cm^2 in order to obtain sufficient particulates for cascade impactor sampling. The results of these tests are presented in Tables 2 and 3 and in Figures 5 through 11.

Curves of sample weight loss for nonflaming combustion of the polyphosphazene material are shown in Fig. 5 for heating rates of 5 and 7.5 W/cm^2. Peak mass loss rates obtained from these curves are given in Table 2. Sample weight loss histories using the force transducer could not be obtained during the flaming tests, because the sample expanded and bulged up to contact the pilot burner tube which interfered with the weight loss measurement. This problem was circumvented during the nonflaming tests

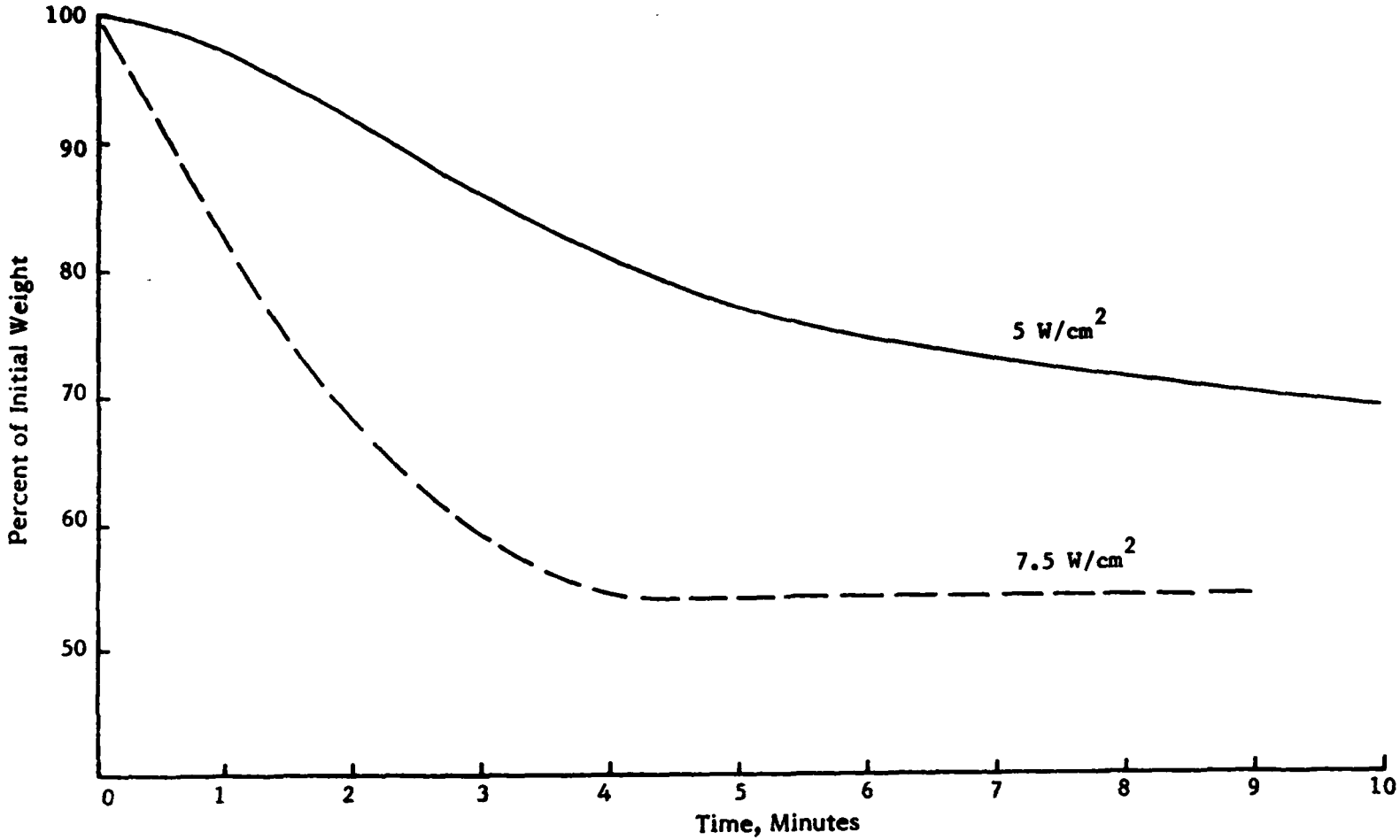

Figure 5. Effect of radiant flux on sample weight losses for nonflaming combustion of polyphosphazene insulation material in room temperature ventilation air (25°C).

Table 2. Sample Weight Loss Data for Polyphosphazene Foam Insulation Material.

Mode	Ventilation Air Temperature (°C)	Radiant Flux (W/cm^2)	Peak Mass Loss Rate (mg/cm^2-s)	Char Residue (% of Initial Weight)
NF	25	5	0.16	66.9
NF	25	7.5	0.52	53.8
NF	100	5	0.22	63.1
NF	300	5	0.52	55.6
F	25	5	Not Available	63.7
F	100	5	Not Available	58.7
F	300	5	Not Available	51.9

by removing the pilot burner tube. The amounts of char residue (Table 2) were obtained for both flaming and nonflaming combustion by weighing the char and comparing with the initial sample weight. As expected, Figure 5 and Table 2 show that the mass loss rate due to pyrolysis under nonflaming conditions increases dramatically as the radiant heat flux is increased. The peak mass loss rate obtained at 7.5 W/cm^2 is over three times the peak rate obtained for 5 W/cm^2. In addition, there was considerably less char residue remaining after the test for the sample exposed to 7.5 W/cm^2 than for the sample exposed to 5 W/cm^2, which indicates that a greater amount of material is pyrolyzed at the higher heating rate. For the room temperature tests conducted at 5 W/cm^2, only slightly less char was produced when flaming combustion occurred. This may be due to the fact that flaming combustion was brief and intermittent during tests of this fire retarded material. During the room temperature tests, the samples were found to expand to about 2.5 times their original volume, forming a black porous char with many cracks in the upper surface as shown in Figure 6.

Smoke particle size distribution measurements were attempted using cascade impactor sampling for all room temperature tests. For both flaming and nonflaming tests conducted at 5 W/cm^2 the amount of particulates collected was too small for determination of the particle size distribution. For nonflaming combustion at 5 W/cm^2, about 95% (by mass) of the particles passed through the cascade impactor and were collected on the absolute filter, while the remaining particles (about 0.3 mg) were collected on the last stage of the cascade impactor (.43-.65 μm). For flaming combustion, about 70% of the particulate mass (about 4 mg) was collected on the filter, while slightly less than 1 mg of particles were collected on each of the last two stages (.43-.65 μm and .65-1.1 μm). Black sooty material was easily visible on the next two stages (1.1-2.1 μm and 2.1-3.3μ m), but was not enough for accurate weight determination (less than 0.1 mg).

A smoke particle size distribution was obtained for nonflaming combustion of the polyphosphazene material at the higher radiant flux of 7.5

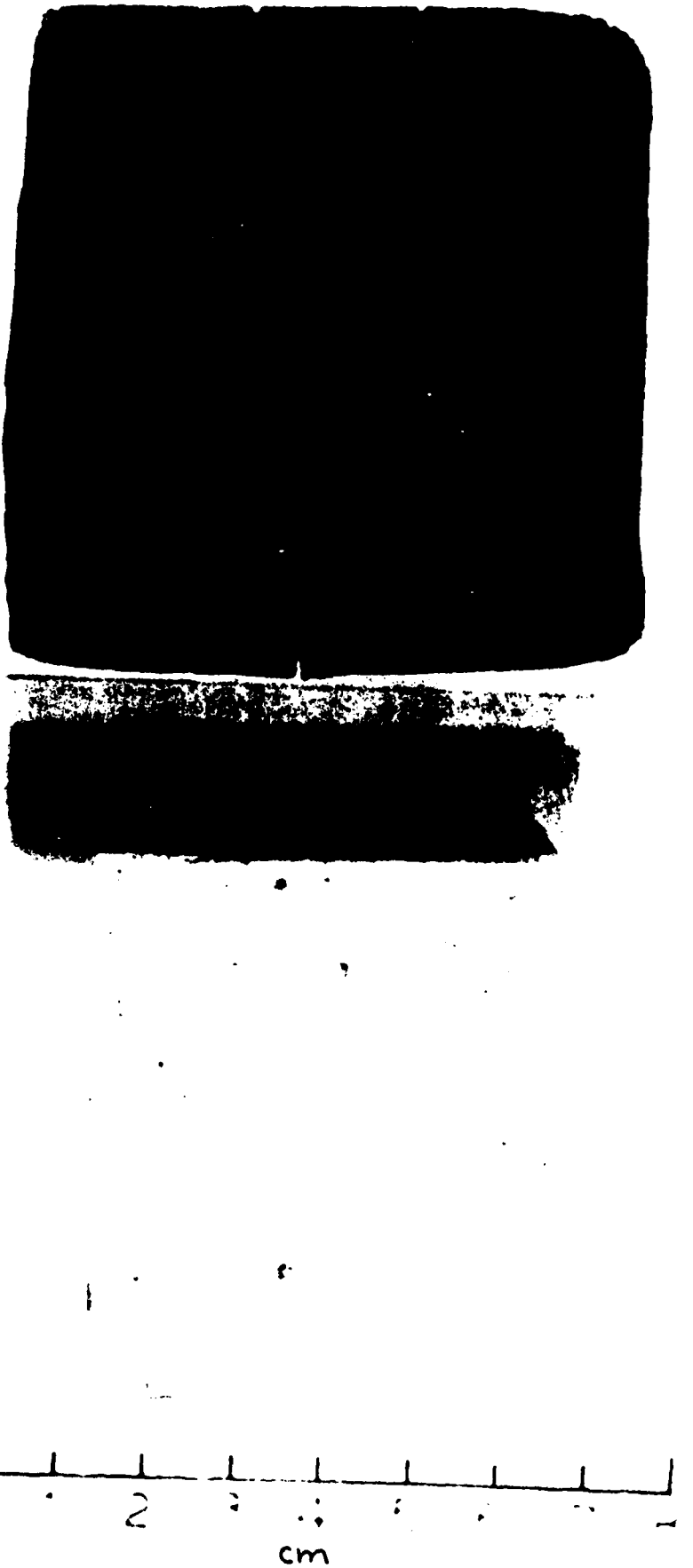

Figure 6. *Polyphosphazene specimen and char for nonflaming combustion under 5 W/cm² radiant flux in room temperature air.*

W/cm^2. This size distribution is shown in Fig. 7 as a cumulative curve generated by plotting the percentage of particulate weight having particle diameters less than a given particle size versus the particle size on log-normal probability coordinates. A straight line gives a good fit to the cascade impactor data (plotted points), which indicates that the size distribution is log-normal. The mass median diameter (D_{MMD}) and standard deviation (σ_g) obtained from this curve are given in Table 3. Most of the sample collected at this heating rate was on the filter (about 8 mg) and the last two stages of the cascade impactor (.43-.65 μm: about 8 mg, .65-1.1 μm: about 6 mg). The cascade impactor sample appeared as a yellowish liquid containing small dark brown particles, while the sample on the filter was a uniform dingy yellow color with no brown material. Another test conducted using only the filter for particulate sampling yielded about 17 mg of a tan material with sprinklings and clusterings of fine brown particles. These results indicate that the particulates produced during nonflaming combustion of the polyphosphazene material at the higher heating rates are a mixture of at least two types of particles: a yellowish liquid with sizes ranging from below 0.2 μm to about 1.5 μm and a much darker, brown, possibly solid material ranging in size from about 0.4 μm to a little over 1.0 μm. Since the samples are collected over a period of several minutes, it is possible that the two types of particulates are produced during different portions of the test.

Sampling data was also used to determine the fraction of the sample mass loss converted to particulates (Γ) for the room temperature tests. These values of Γ are given in Table 3, which show that the largest value of Γ was obtained for nonflaming combustion under 7.5 W/cm^2 radiant flux. At 5 W/cm^2 the values of Γ obtained under flaming and nonflaming conditions were about the same. This latter result is probably due to the brief and intermittent flaming obtained for this material.

The in situ optical system was used to determine the variation of mean particle diameter (D_{32}) and optical density during each of the

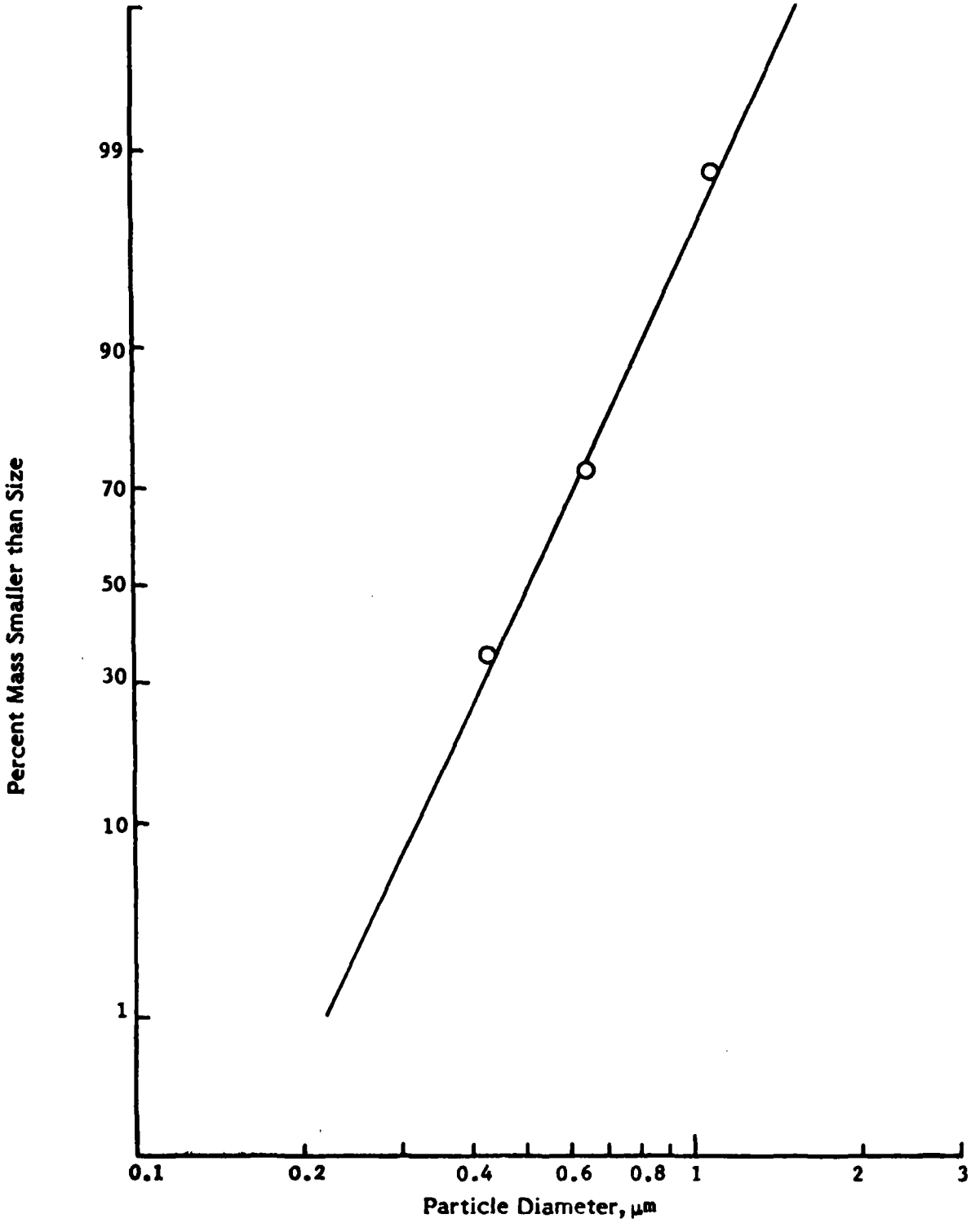

Figure 7. Smoke particle size distribution for nonflaming combustion of polyphosphazene insulation material exposed to a radiant flux of 7.5 W/cm^2 in room temperature ventilation air (25°C)

polyphosphazene burns. The effect of radiant flux upon the mean particle sizes and optical densities for room temperature nonflaming polyphosphazene tests are given in Figures 8 and 9. Peak optical densities, the corresponding value of D_{32} at peak optical density, and the time required to reach peak optical density are presented in Table 3. From Figure 8, it is seen that, although D_{32} is initially about 1 micron, mean particle size drops rapidly to about 0.4 micron during the first two minutes of the test. At 7.5 W/cm^2 the initial decline in mean particle size is more rapid and there is less variation in D_{32} during the rest of the test than at 5 W/cm^2. For the 7.5 W/cm^2 case, the values of D_{32} determined optically are in excellent agreement with the mass median diameter (D_{MMD}) obtained from the cascade impactor sample (Table 3). Figure 9 shows that radiant heating flux has a strong effect on the optical density of the smoke particulates for nonflaming combustion. The peak optical density at the blue-green argon-ion laser line (0.488 μm) obtained for tests at 7.5 W/cm^2 is about six times greater than that obtained at 5 W/cm^2. Also the optical density peak is sharp and occurs early in the 7.5 W/cm^2 tests, while the peak is broad and occurs during the middle of the 5 W/cm^2 tests. This behavior is believed to be due to the much larger weight loss (pyrolysis) rate (Table 2) and larger value of Γ (Table 3) obtained at the higher radiant heating rate, which results in a much larger concentration of smoke particulates for this case.

Mean particle diameters and optical densities for flaming combustion of the polyphosphazene insulation material are compared with the corresponding data for nonflaming combustion in Figures 10 and 11. Figure 10 shows that the largest particles are produced during a brief period of flaming combustion, with D_{32} reaching a peak of about 1.1 micron immediately after flaming ignition (between one and two minutes after exposure to 5 W/cm^2 radiant flux and the pilot flame). After about 20 seconds of strong flaming combustion involving the entire sample surface, D_{32} declines to values between 0.6 and 0.8 micron for the remainder of the test. During this latter period a weak intermittent flame is observed. As shown in Figure 11, this brief period of strong flaming combustion coincides

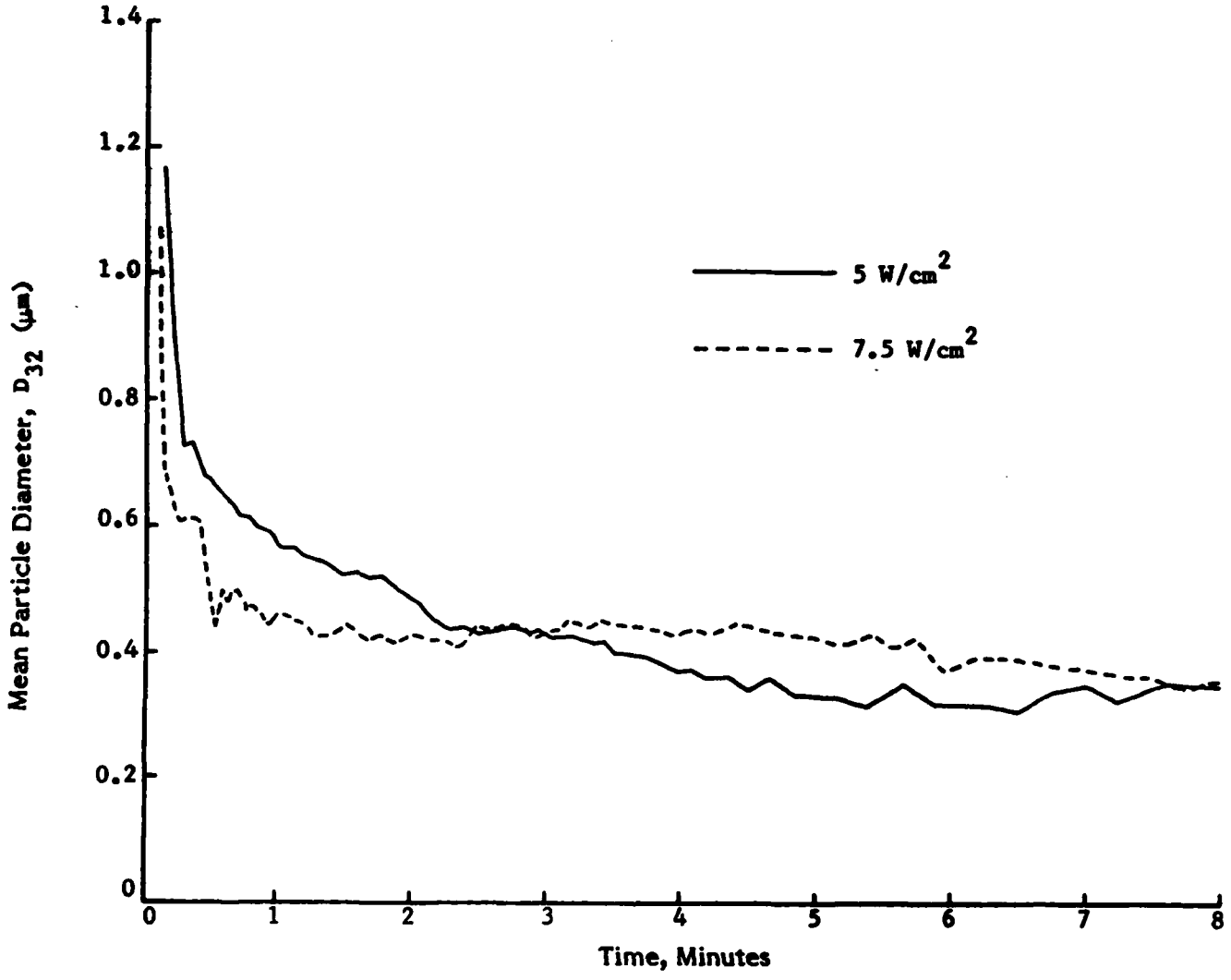

Figure 8. Effect of radiant flux on smoke mean particle diameters for nonflaming combustion of polyphosphazene insulation material in room temperature ventilation air(25°C).

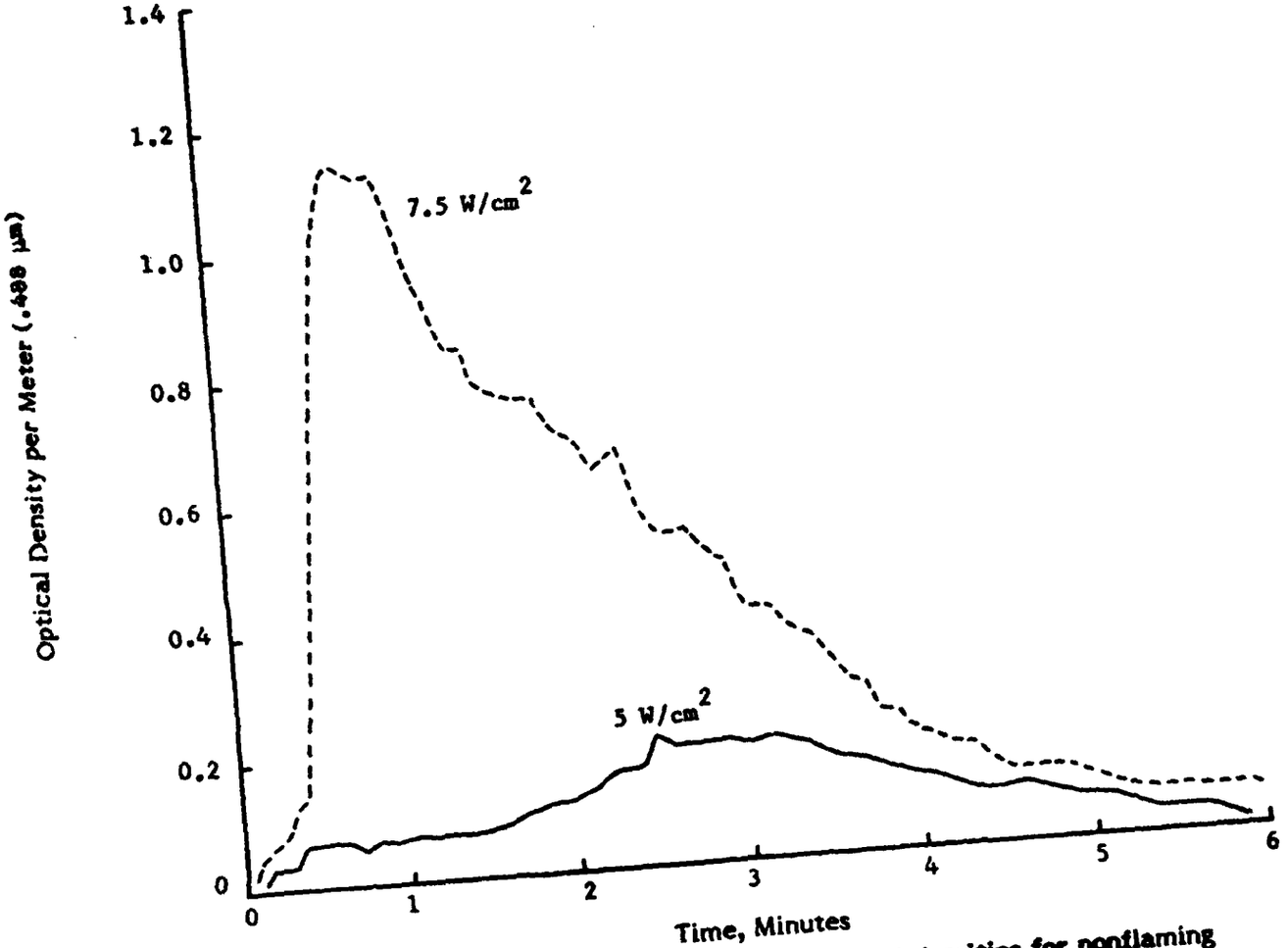

Figure 9. Effect of radiant flux on smoke optical densities for nonflaming combustion of polyphosphazene insulation material in room temperature ventilation air (25°C).

Table 3. Smoke Properties Data for Polyphosphazene Wall Insulation Material.

Mode	T (°C)	Radiant Flux (W/cm^2)	Γ	D_{MMD} (μm)	σ_g	OD_{max} (m^{-1}) Blue	OD_{max} (m^{-1}) Red	D_{32}* (μm)	Time to Peak OD (min)
NF	25	5	.019			0.21	0.10	0.39	3.3
NF	25	7.5	.046	0.51	1.44	1.23	0.79	0.47	0.9
NF	100	5				0.24	0.17	0.42	2.4
NF	300	5				0.56[a]	0.27[a]		1.1
F	25	5	.017			0.64	0.49	1.07	1.7
F	100	5				0.56	0.51	1.12	1.1
F	300	5				1.17[b]	0.90[b]	1.17	0.5

* Average of data points near OD_{max}.

a Attributed to gas phase absorption, no measurable scattered light.

b First and largest of two peaks.

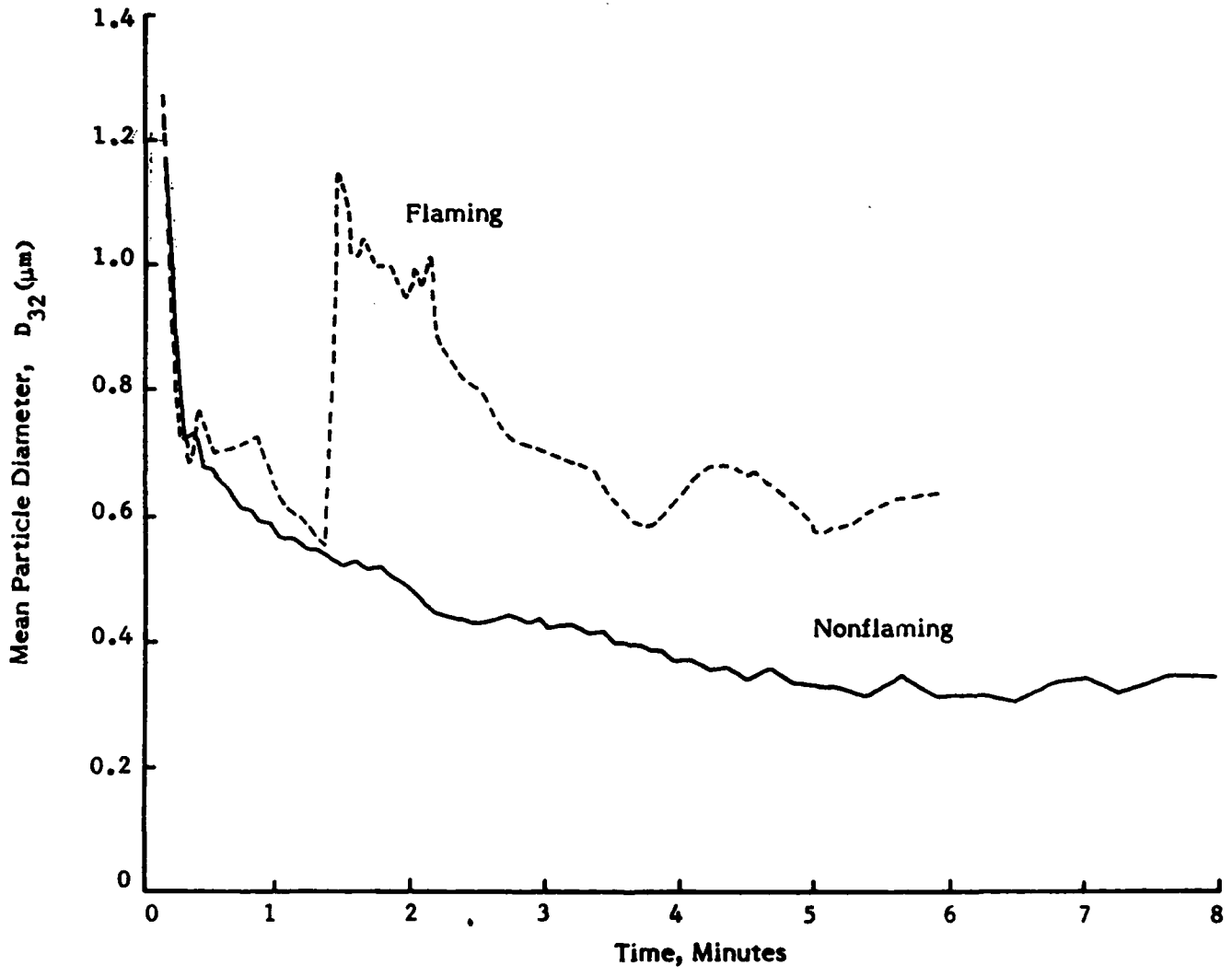

Figure 10. Smoke mean particle diameters for flaming and nonflaming combustion of polyphosphazene insulation material exposed to a radiant flux of 5 W/cm^2 in room-temperature ventilation air (25°C).

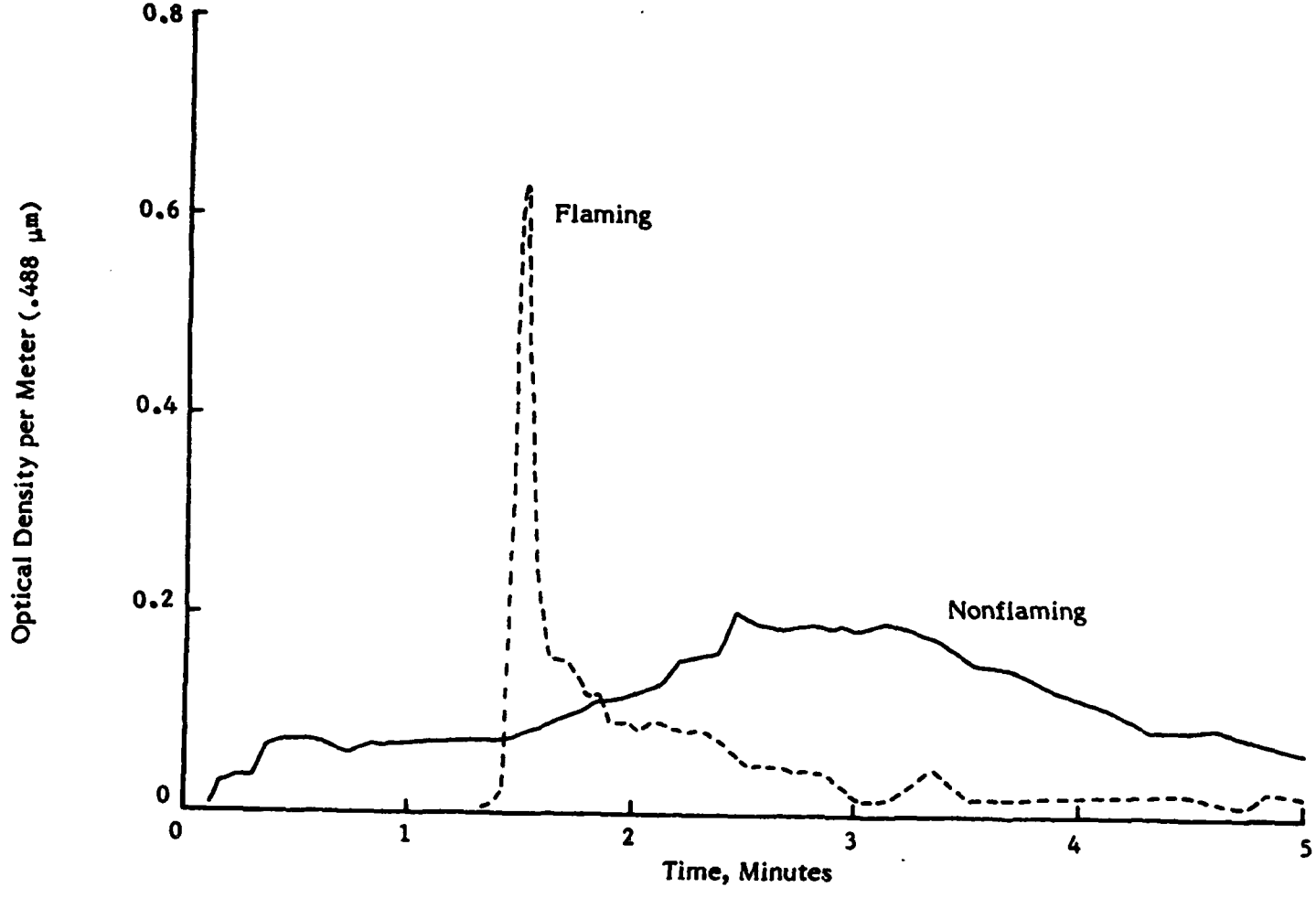

Figure 11. Smoke optical densities for flaming and nonflaming combustion of polyphosphazene insulation material exposed to a radiant flux of 5 W/cm^2 in room temperature ventilation air (25°C).

with the sharp spike in the optical density curve, which reaches a peak optical density of about 0.6 m^{-1}. During this period heavy black smoke is observed. Thereafter the optical density rapidly falls below the values obtained during nonflaming combustion. This is consistent with the rapid depletion of combustible pyrolysis products during the flaming phase, after which the concentration of combustible gases is low and only a weak flame and little soot is produced.

Tests in Heated Ventilation Air

Results of tests of polyphosphazene wall insulation material conducted in hot ventilation air are shown in Figs. 12 through 14 for nonflaming combustion and in Figs. 15 and 16 for flaming combustion. In each figure the room temperature data are also shown for comparison. High temperature data are also given in Tables 2 and 3. In all cases the radiant flux is 5 W/cm^2.

Figure 12 and Table 2 show that, for nonflaming combustion of the polyphosphazene material, increasing the ventilation air temperature increases the peak mass loss rates and decreases the amount of char residue. The peak mass loss rate obtained at 300°C is over three times that obtained in the room temperature tests, while the total mass lost during combustion is about 33% greater at 300°C than at room temperature. The peak mass loss rate also occurs earlier in the test at higher ventilation air temperatures. For 300°C ventilation air, half of the mass loss has occurred by 1.7 minutes after initiation of exposure, while 3.4 minutes are required for a similar mass loss to occur in the room temperature environment. Weight loss rate data for flaming tests in heated ventilation air could not be obtained for the same reasons as noted previously for room temperature tests. However, Table 2 shows that the amount of char residue also decreases with increasing temperature for flaming combustion. Furthermore, at each temperature the amount of char residue was less for flaming than for nonflaming combustion. All of these results are consistent

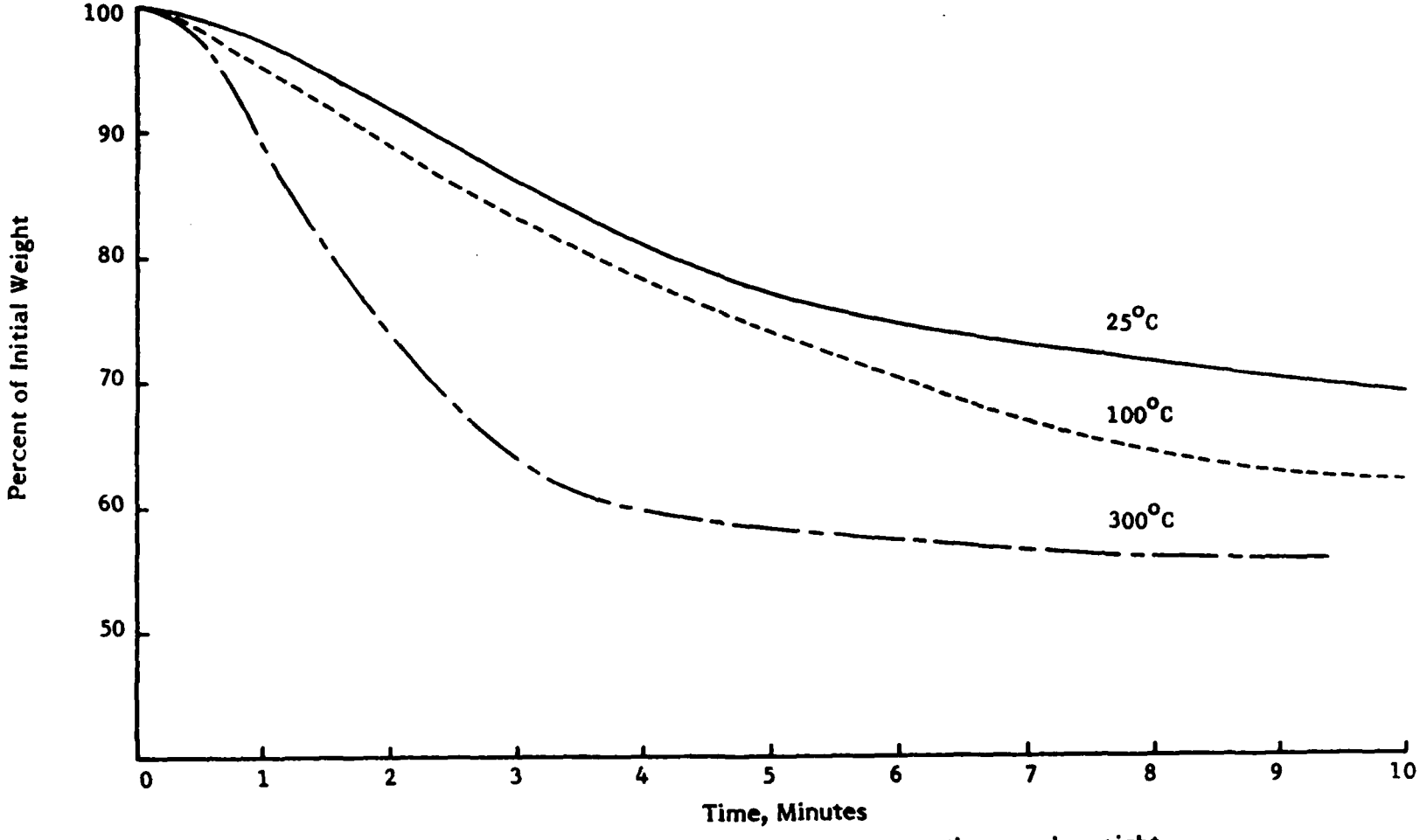

Figure 12. Effect of the ventilation air temperature on the sample weight loss for nonflaming combustion of polyphosphazene insulation material exposed to a radiant flux of 5 W/cm^2.

with increased heat transfer to the sample from the hot ventilation gas and the flame (if present), which results in increased pyrolysis rates and greater amounts of material pyrolyzed.

Mean particle diameters for nonflaming tests conducted in room temperature and 100°C atmospheres are compared in Fig. 13. The initial production of larger particles, which is characteristic of the room temperature tests, does not occur at the higher temperature. Thus these first particles, which range from 0.6 to 1.2 microns (D_{32}), consist of a substance (possibly water) with a boiling point less than or equal to 100°C. For the 100°C test, mean particle diameter decreases only slightly during the five minute test, always being close to 0.4 micron. As can be seen from Table 3, the mean particle diameter corresponding to the peak optical density is nearly the same for both room temperature and 100°C tests. For nonflaming tests conducted at 300°C, no forward scattered light was detected. This indicates that little or no particulates are produced during nonflaming combustion of this polyphosphazene formulation at environmental temperatures above 300°C. Thus it appears that the pyrolysis products from the polyphosphazene insulation material contain very little or no compounds with boiling points above 300°C and that most of the particulates consist of substances with boiling points between 100°C and 300°C.

Figure 14 shows the effect of ventilation air temperature upon optical density (λ = .488 μm) during nonflaming tests of the polyphosphazene insulation material. The curves in Fig. 14 are based on directly measured values, while the corresponding peak optical densities (λ = .488 μm and .633 μm) given in Table 3 have been corrected for the higher ventilation air flow rates obtained at higher temperatures (see Eq. (A-4) of Appendix A). This data shows that for moderate increases in temperature, the rather broad optical density peak occurs somewhat earlier, but the maximum optical density remains about the same. For ventilation air at 300°C, however, the optical density increases rapidly to a sharp maximum (corrected) which is nearly three times that obtained during room

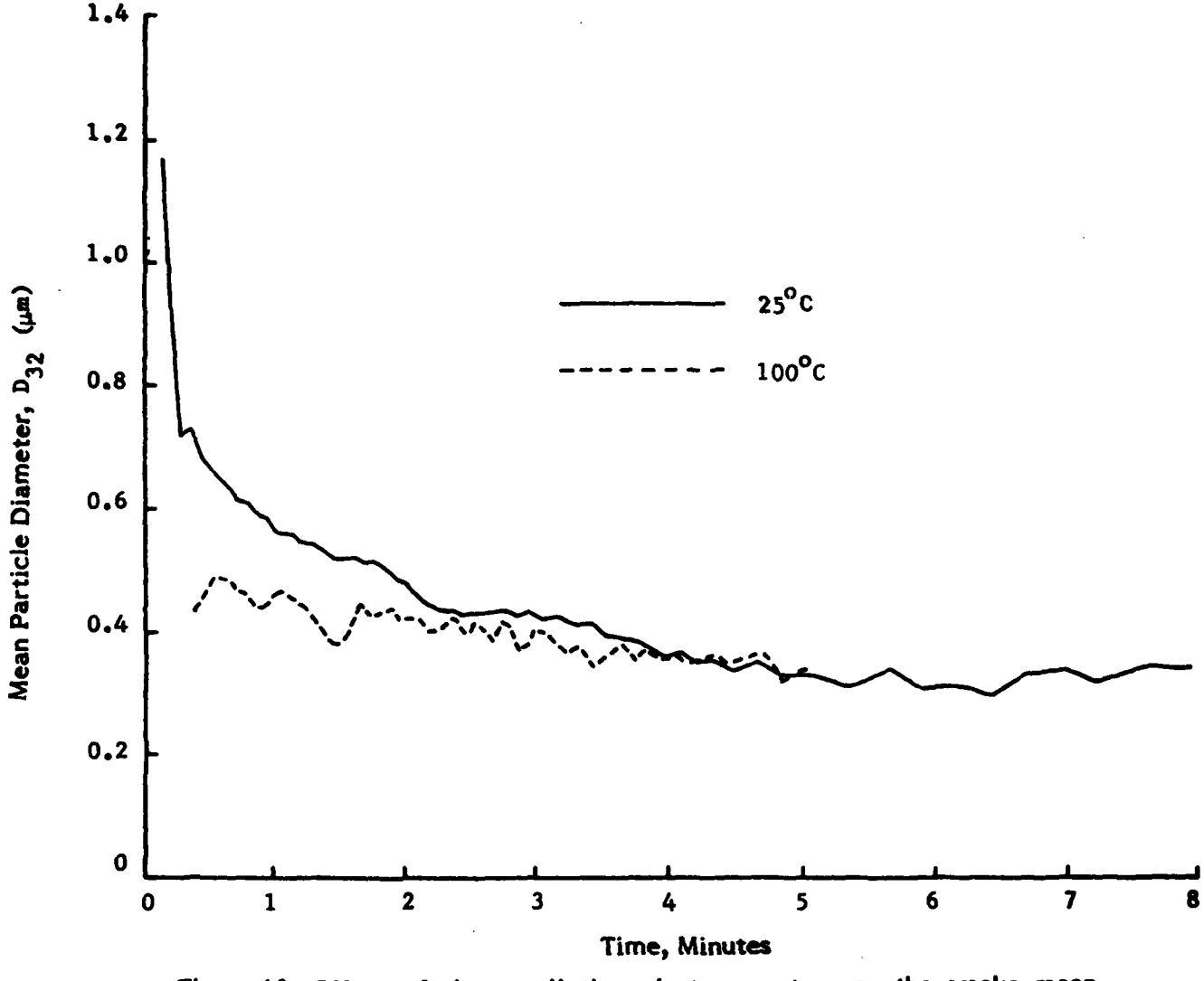

Figure 13. Effect of the ventilation air temperature on the smoke mean particle diameter for nonflaming combustion of polyphosphazene insulation material exposed to a radiant flux of 5 W/cm^2.

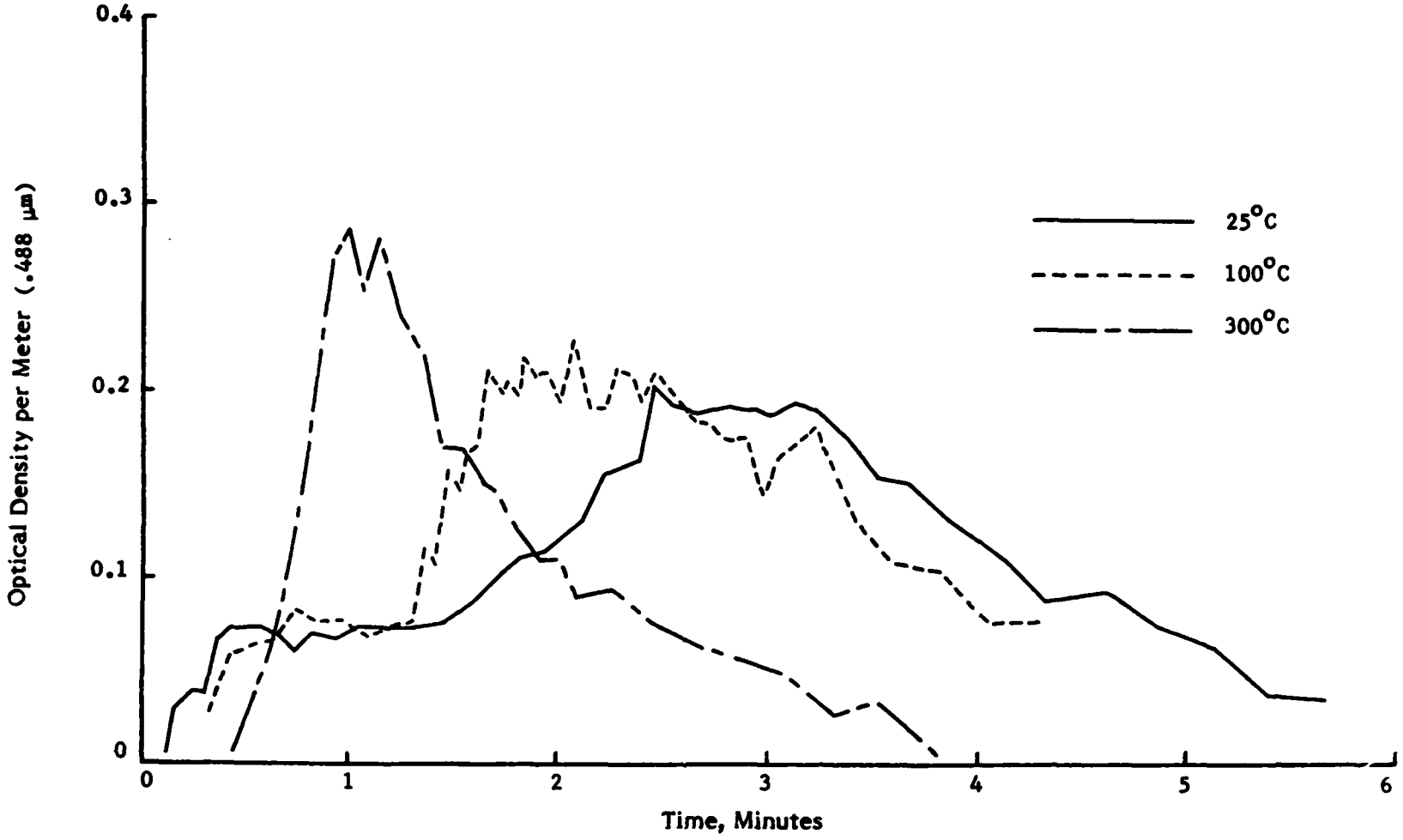

Figure 14. Effect of the ventilation air temperature on the smoke optical density for nonflaming combustion of polyphosphazene insulation material exposed to a radiant flux of 5 W/cm^2.

temperature tests. Since there was no scattered light detected at 300°C, this optical density is probably due to absorption of light by gaseous pyrolysis products. It is also possible that gas phase absorption may contribute to the optical density measured at lower temperatures. If this is indeed the case, the values of the particulate volume fractions computed from the measured optical densities will be too large.

The effect of ventilation air temperature upon the mean particle diameters obtained during flaming combustion of the polyphosphazene material is shown in Fig. 15. At room temperature and at 100°C, a sharp rise in particle size occurs upon flaming ignition. Although the pilot flame is ignited at t = 0, the sample does not ignite until about a minute later when sufficient pyrolysis products are evolved to form a combustible mixture. As expected this ignition delay is somewhat shorter at 100°C than at room temperature. At 300°C, flaming ignition occurs almost immediately and lasts about two minutes during which mean particle size fluctuates about 1.2 microns. Figure 15 and Table 3 show a definite trend of increasing mean particle diameter D_{32} as the ventilation air temperature is increased. This behavior has been observed previously for a variety of materials such as Douglas fir and rigid PVC [5], PVC cable jacket and PVC nitrile rubber insulation [6]. A possible explanation of this behavior is that at higher ventilation air temperatures the temperature in the reaction zone of the diffusion flame, the rate of production of pyrolysis products (fuel) and the temperature in the soot production zone on the fuel side of the flame are all increased while the mass flow rate of oxidizer (air) remains fixed. It has been demonstrated experimentally that increasing the temperature of diffusion flames generally leads to greater quantities of soot particles produced in the flame [7]. This enhances the agglomeration process in the smoke plume, which accounts for the larger particle sizes observed.

Curves of optical density variation with time for flaming combustion of the polyphosphazene material at different environmental temperatures are presented in Fig. 16. At room temperature and at 100°C, the optical

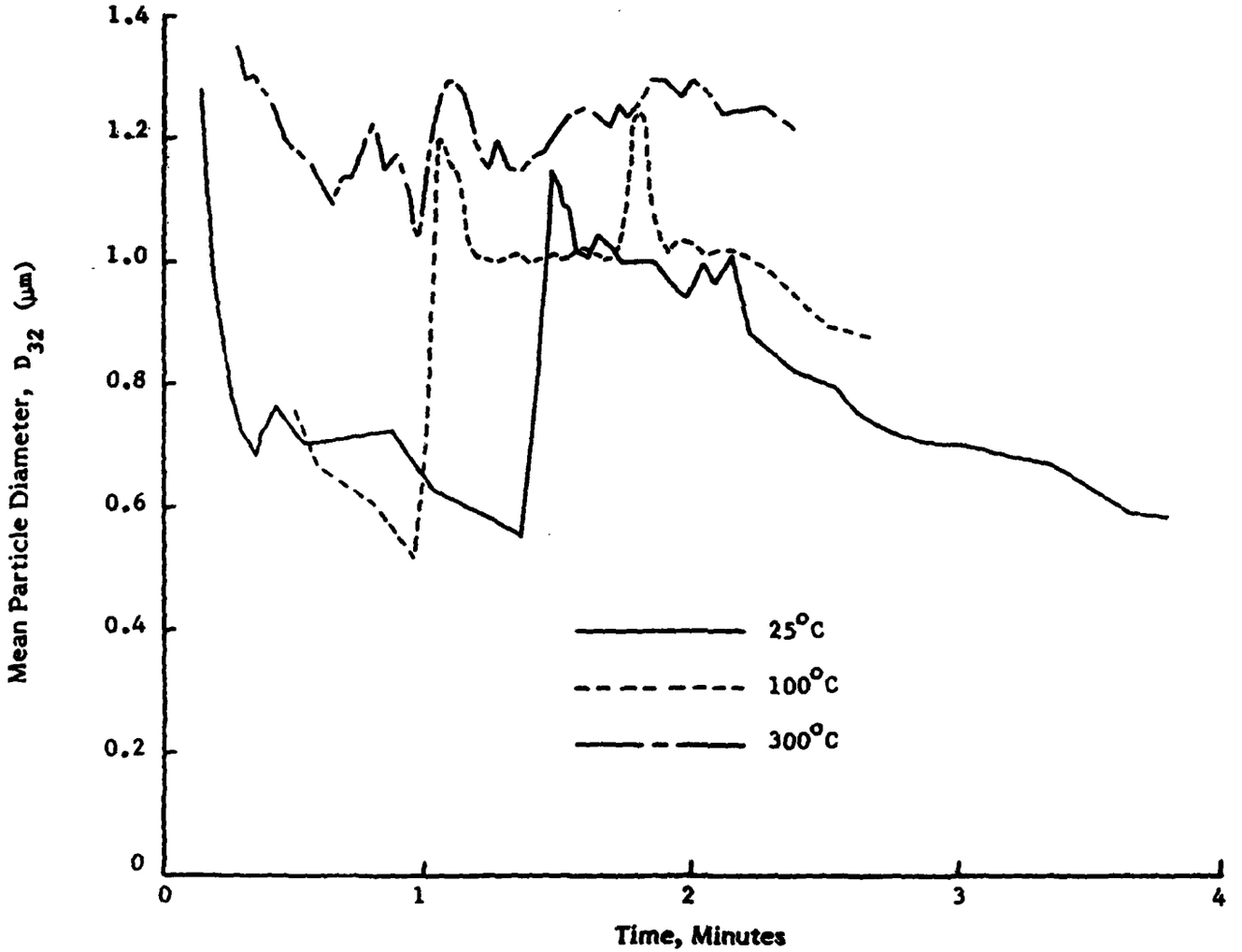

Figure 15. **Effect of the ventilation air temperature on the smoke mean particle diameter for flaming combustion of polyphosphazene insulation material exposed to a radiant flux of 5 W/cm^2.**

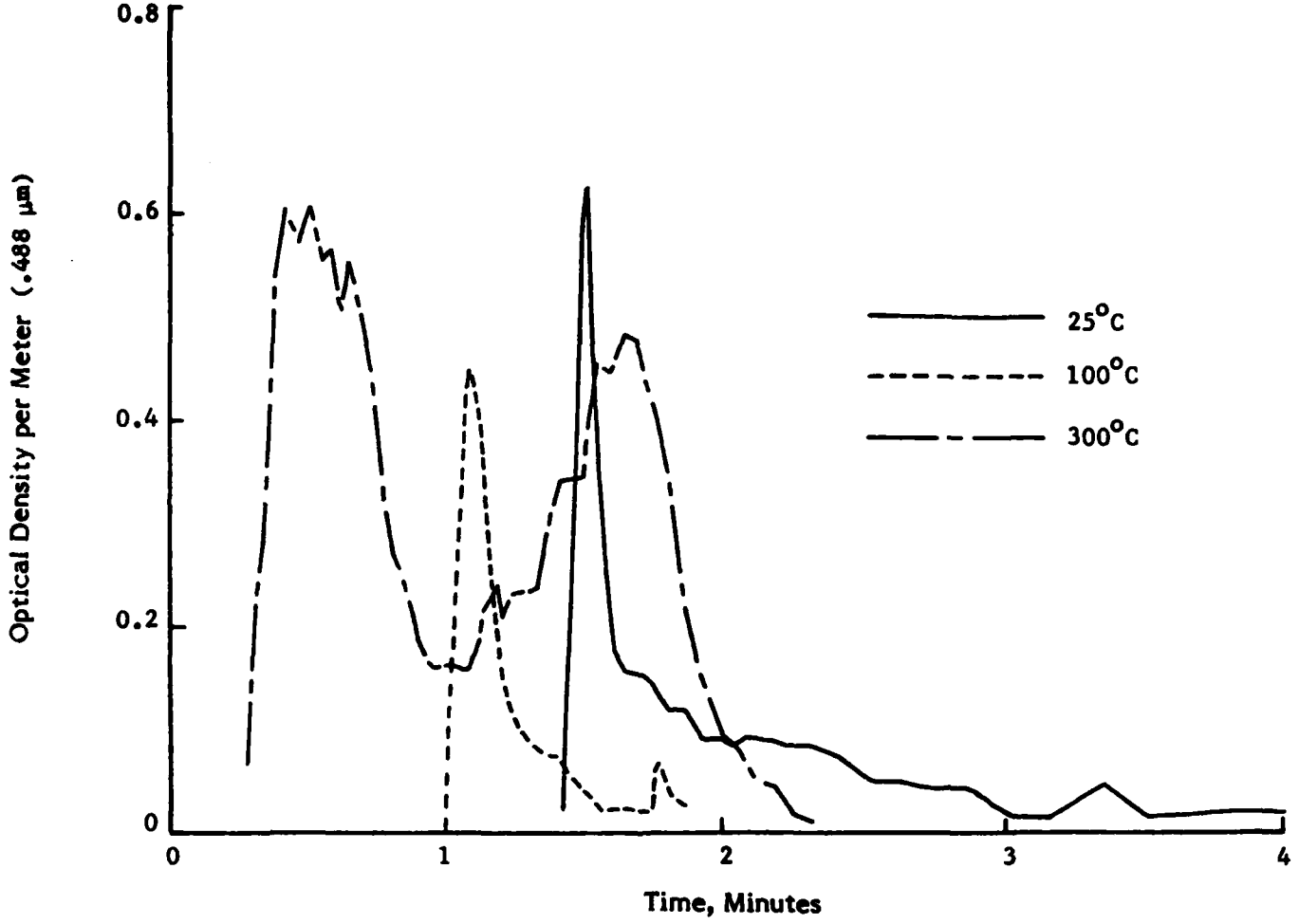

Figure 16. Effect of the ventilation air temperature on the smoke optical density for flaming combustion of polyphosphazene insulation material exposed to a radiant flux of 5 W/cm^2.

density rises rapidly upon flaming ignition (in a few seconds) to a narrow peak between 0.4 and 0.6 m^{-1} and then falls nearly as rapidly to levels below 0.2 m^{-1} at the end of flaming combustion. The width of this peak is less than 10 seconds at the half-peak height. During the remaining time only intermittent flickering flaming occurs and the optical density is low and gradually declining. At 300°C the optical density curves are quite different. Upon ignition the optical density rises rapidly to about 0.6 m^{-1} as at the lower temperatures, but the peak is much wider and a second strong peak (0.5 m^{-1}) occurs about a minute after the first one. Between these peaks the optical density drops to about a third of its peak value. This behavior indicates that at 300°C, flaming combustion of the polyphosphazene material is much more vigorous than at the lower temperatures, and that two periods of strong flaming combustion occur separated by an interval of weaker combustion. When the temperature corrections are applied (see Table 3), moderate increases of environmental temperature (i.e. to 100°C) have little effect on peak optical density at either wavelength. Increasing the ventilation air temperature to 300°C, however, results in a doubling of the peak optical density and dramatically increases the length of time during which significant light obscuration by smoke occurs.

Smoke Particle Refractive Index and Volume Fraction.

For nonflaming tests of the polyphosphazene insulation material, measurements of the ratio of optical densities, OD_R/OD_B, and the 90-degree scattering ratio, $I_{\parallel}/I_{\perp}$, were used to determine the complex refractive index of the smoke particles. For each test, it was initially assumed that the particles were nonabsorbing (k = 0), and the measured values of $I_{\parallel}/I_{\perp}$ in blue-green light (λ = .488 μm) along with the previously determined values of D_{32} were used to calculate the corresponding refractive index n_B. For the room temperature test at 7.5 W/cm^2, measured OD_R/OD_B values were also used to obtain the refractive index, assuming that k = 0 and that n does not vary significantly with wavelength. These latter calculations were not performed for tests conducted at 5 W/cm^2,

since the optical densities obtained were too low for reliable measurements of OD_R/OD_B.

Calculated values of n_B from the 90°-degree scattering data reveal considerable variations in refractive index with time during a test, as shown in Fig. 17 for the room temperature test at 7.5 W/cm^2. For this case the refractive index exhibits a sharp initial peak (n_B = 1.50) followed by a decline to about 1.38 and a gradual rise to about 1.45. Such variations in refractive index indicate corresponding variations in the chemical composition of the smoke particles during the test. Near the time of peak optical density, average values of n_B and n_R of 1.41 were obtained from the optical density ratio, OD_R/OD_B, while the corresponding value of n_B from $I_\parallel/I_\perp$ was 1.45. In order to reconcile these two values, the assumption of $k = 0$ was relaxed and the Mie theory was used in an attempt to determine n and k to simultaneously satisfy the OD_R/OD_B and $I_\parallel/I_\perp$ data. This proved to be impossible for most of the data, requiring a negative value of k for a solution. A different approach was then taken by requiring that $k = 0$, but allowing n to vary with wavelength. In this method, n_R was calculated from the measured OD_R/OD_B values using the values of n_B obtained previously from the $I_\parallel/I_\perp$ data. This method was successful in fitting both the OD_R/OD_B and $I_\parallel/I_\perp$ data. As shown in Fig. 17, the refractive index in red light (λ = .633 μm) is slightly smaller than the refractive index in blue-green light (λ = .488 μm), and it exhibits similar variations with time during the test. The averaged values of the refractive indices at peak optical density are n_B = 1.452 and n_R = 1.439.

The refractive index of the smoke particles produced during nonflaming combustion of the polyphosphazene material was also found to depend upon the radiant heating flux and the ventilation air temperature. The variations in particulate refractive index during tests conducted at room temperature and 100°C under 5 W/cm^2 radiant flux and at room temperature under 7.5 W/cm^2 radiant flux are compared in Figure 18. For room temperature tests, the particulates produced under 5 W/cm^2 have refractive indices n_B considerably lower than those of the particulates

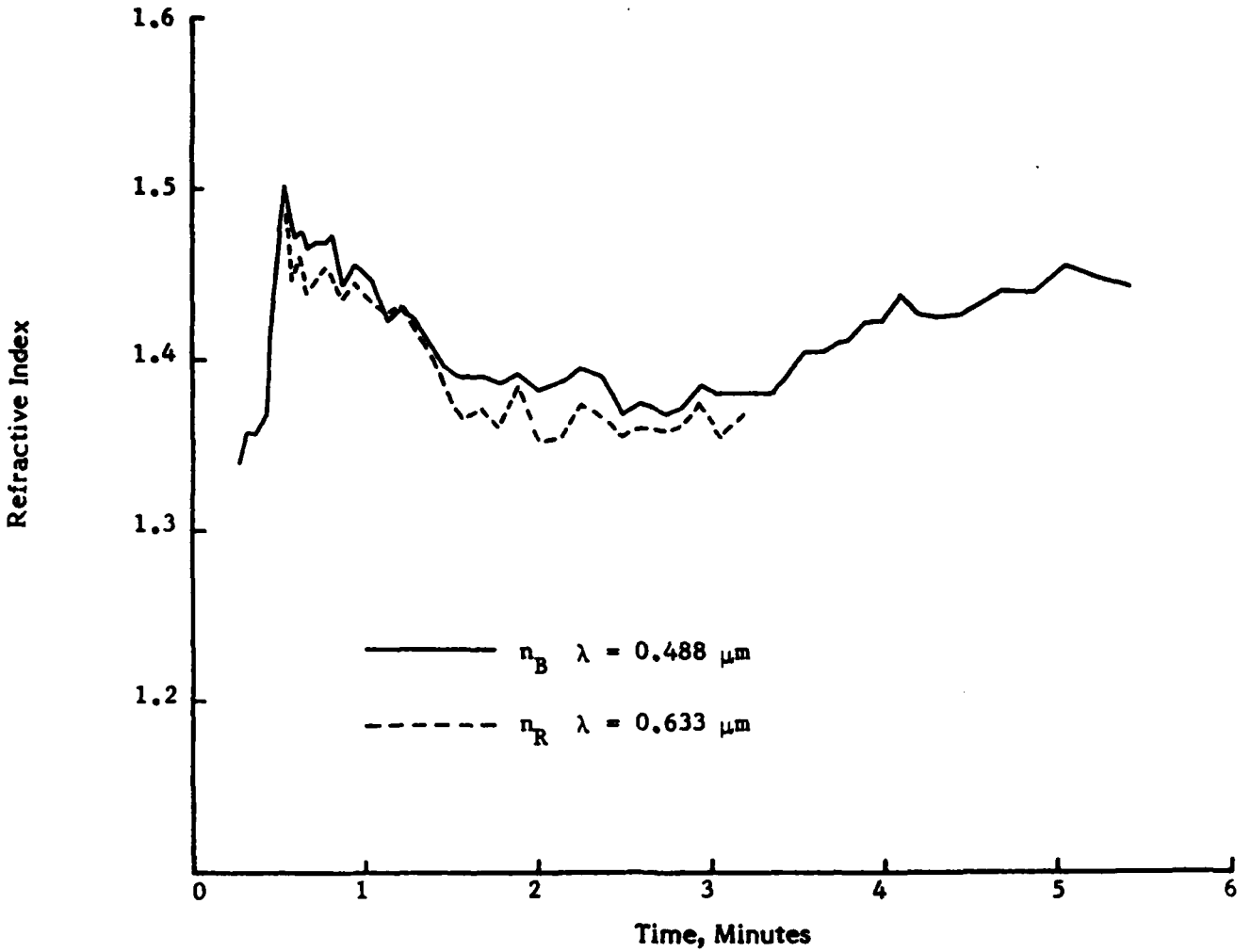

Figure 17. Variation of smoke particle refractive index during nonflaming combustion of polyphosphazene insulation material exposed to a radiant flux of 7.5 W/cm^2 in room temperature ventilation air (25°C).

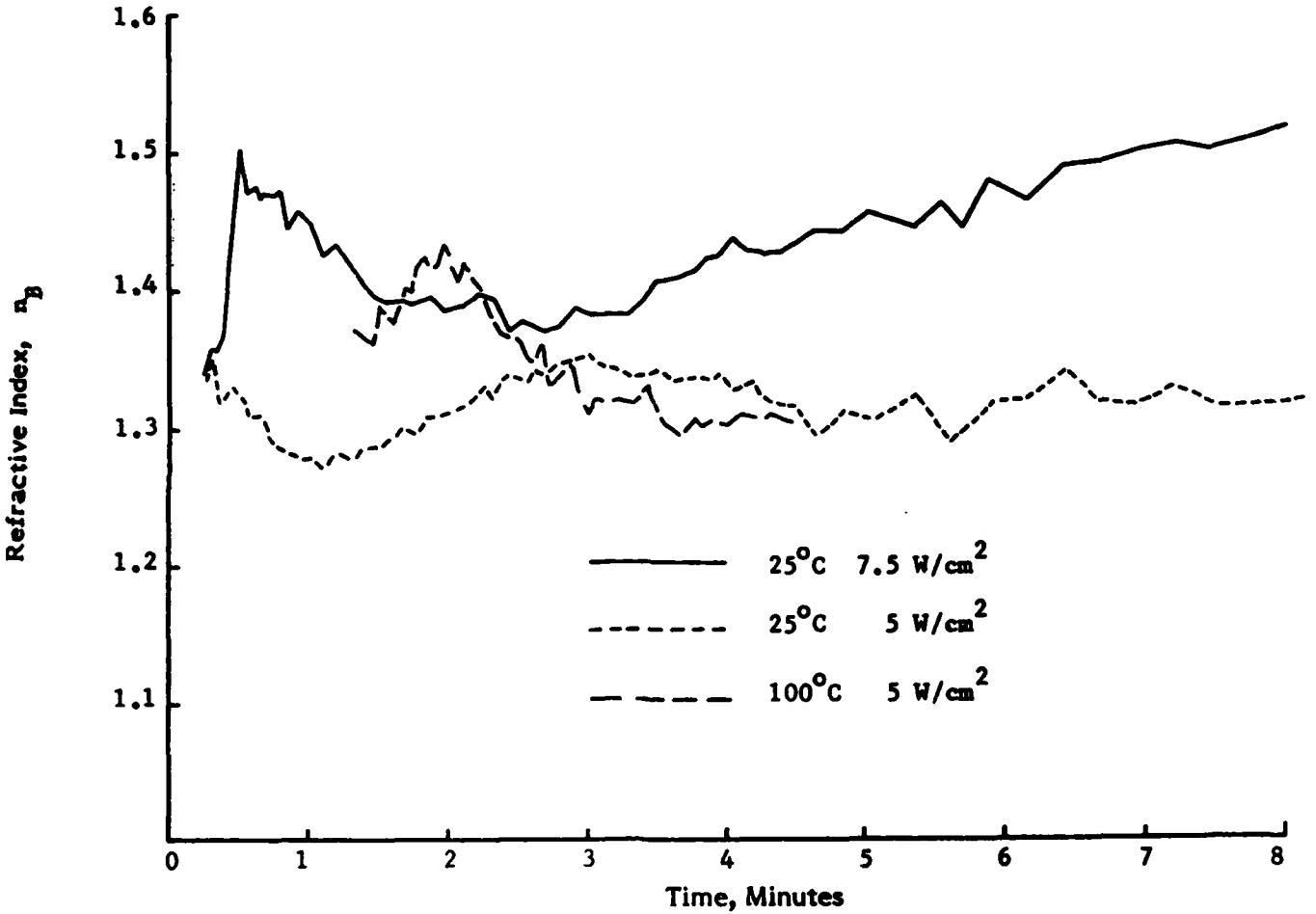

Figure 18. Effects of the ventilation air temperature and the radiant flux on smoke particle refractive index for nonflaming combustion of polyphosphazene insulation material.

generated under the higher radiant flux. This is consistent with the hypothesis that under pyrolysis at the lower radiant flux, the surface temperature is lower and the particulates consist of lighter, more volatile, and less refractive substances (see Appendix B). In fact, the refractive index at peak optical density, n_B = 1.35, for the test at 5 W/cm^2 is only slightly greater than the refractive index of water (n = 1.33). The data for the 100°C case shows that a similar situation exists when the ventilation air temperature is increased (Fig. 18); the lighter and more volatile pyrolysis products remain in the gas phase, while the heavier, less volatile, and more refractive species condense to form smoke particles. Values of the refractive index at maximum optical density are compared in Table 4, which shows that the smoke particle refractive index obtained at 100°C (5 W/cm^2) is intermediate between the refractive indices obtained at 5 W/cm^2 and 7.5 W/cm^2 at room temperature (25°C).

Particulate volume fractions for the nonflaming tests of the polyphosphazene insulation material were calculated using the refractive index values plotted in Fig. 18. The resulting variations in particulate volume fraction (expressed in parts per million, ppm) during these tests are shown in Figure 19. Except for the 300°C case, the shapes of the curves of volume fraction versus time and their dependence on temperature and radiant flux are similar to those of the optical density curves given in Figs. 9 and 14. This shows that the optical density of the smoke is determined principally by its concentration and that variations in particle size and refractive index only play secondary roles. Peak volume fractions for these tests are given in Table 4.

For the case of <u>flaming</u> combustion of the polyphosphazene insulation material, the soot particles produced are highly absorbing, and the determination of the complex refractive index (n and k) from the measured values of OD_R/OD_B and $I_{\parallel}/I_{\perp}$ is difficult and unreliable. Figure 20 shows measured values of $I_{\parallel}/I_{\perp}$ and OD_R/OD_B plotted versus D_{32} for a typical flaming test conducted in room temperature air, while Figure 21 shows

Table 4. Smoke Refractive Index, Volume Fraction, and Total Volume for Polyphosphazene Insulation Material.

Mode	Ventilation Air Temperature (°C)	Radiant Flux (W/cm^2)	Refractive Index	Peak Volume Fraction (ppm)	Specific Total Particle Volume (cm^3/g)	$\frac{\Gamma}{\Gamma_{25}}$
NF	25	5	1.35	.093	.0129	1.00
NF	25	7.5	1.45	.297	.0243	-
NF	100	5	1.39	.073	.0056	0.39
NF	300	5	-	.000	.0000	.00
F	25	5	1.57-.56i	.434	.0047	1.00
F	100	5	1.57-.56i	.402	.0025	0.46
F	300	5	1.57-.56i	.91[a]	.0262	4.2

[a] First of two peaks, second peak of .72 ppm.

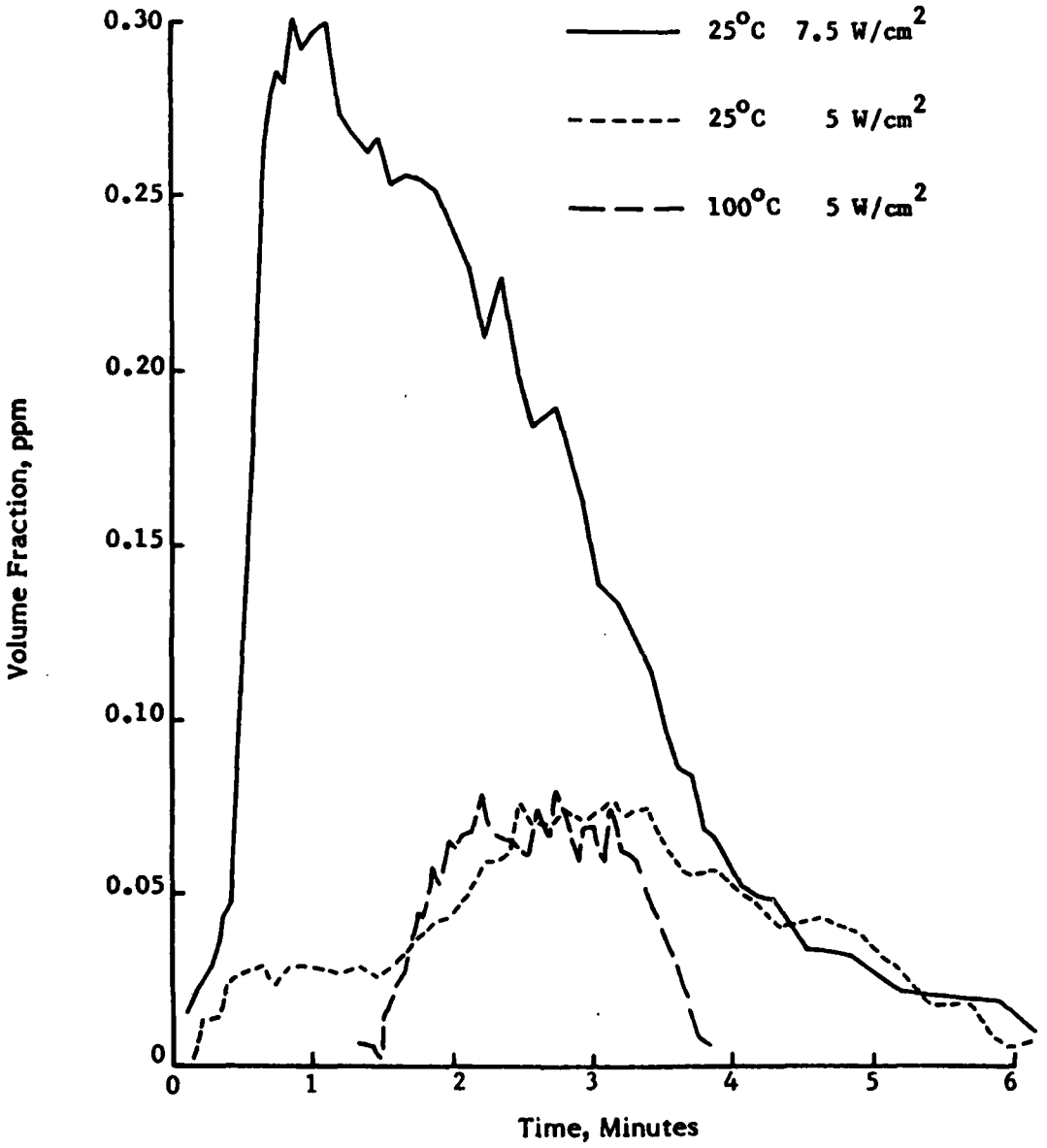

Figure 19. Effects of the ventilation air temperature and radiant flux on the particulate volume fraction for nonflaming combustion of polyphosphazene insulation material.

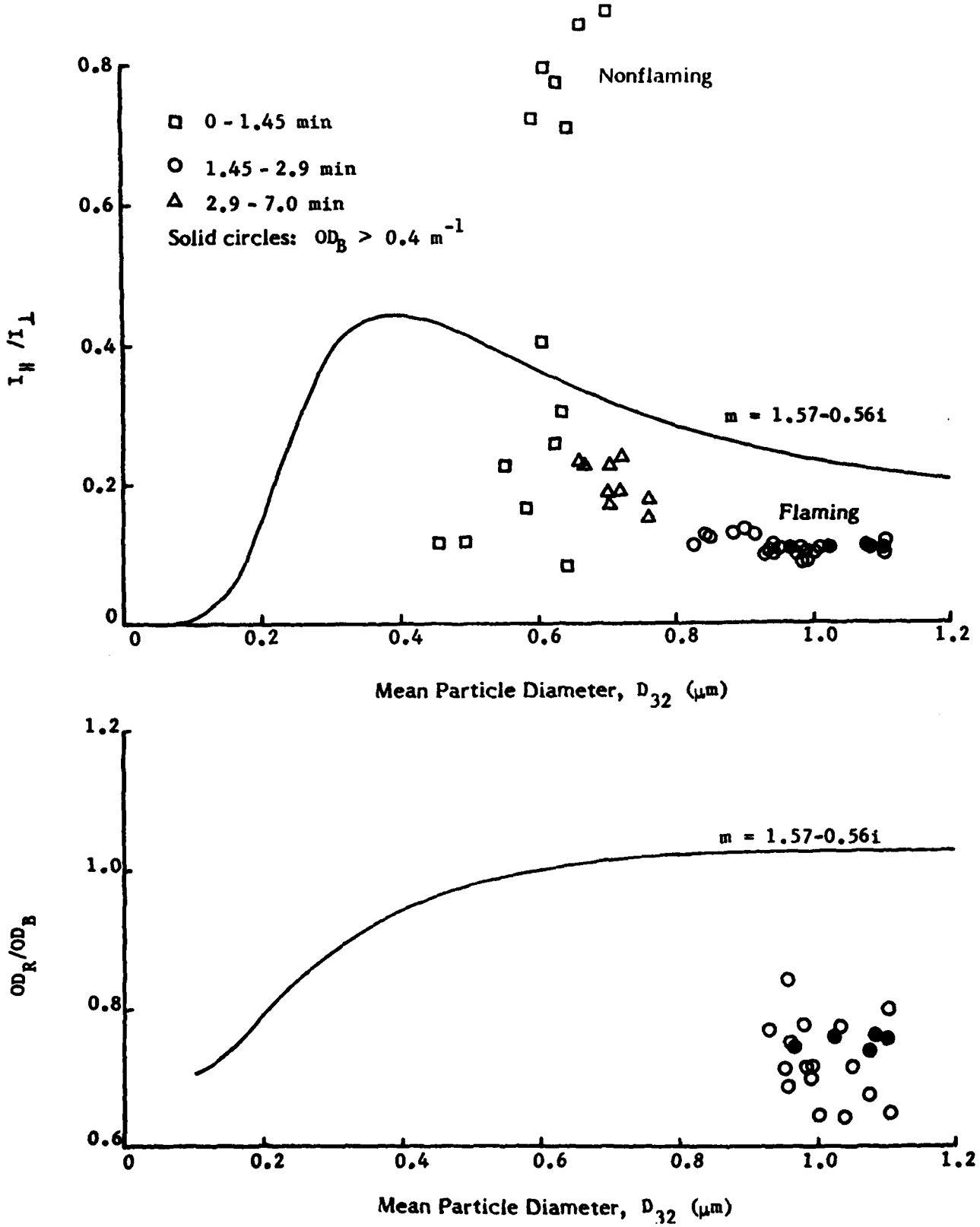

Figure 20. Optical density ratios and 90°-scattering ratios for flaming combustion of polyphosphazene insulation material exposed to a radiant flux of 5 W/ ^{2} in room temperature ventilation air (25°C).

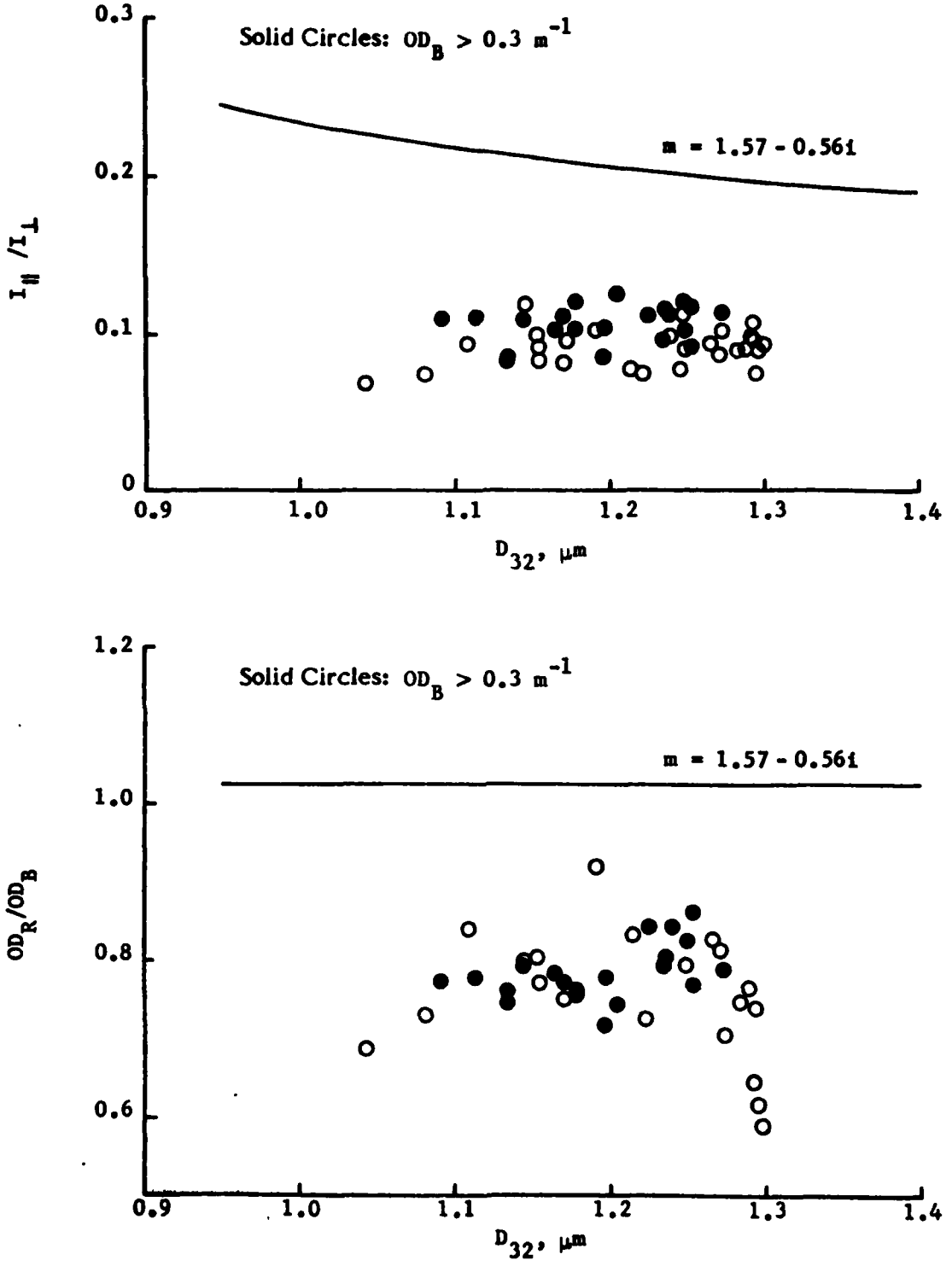

Figure 21. Optical density ratios and 90°-scattering ratios for flaming combustion of polyphosphazene insulation material exposed to a radiant flux of 5 W/cm^2 in 300°C ventilation air.

similar data for a test conducted in 300°C air. Also plotted in Figures 20 and 21 are curves of $I_{\parallel}/I_{\perp}$ and OD_R/OD_B versus D_{32} which were calculated using the Mie scattering theory with m = 1.57 - 0.56i (Dalzell et al [8]). For both 25°C and 300°C tests, the measured values of $I_{\parallel}/I_{\perp}$ are seen to cluster about 0.1 which is about half as large as the theoretical values. This discrepancy is much larger than that obtained previously with PVC-nitrile rubber,[6] where the data could be fitted reasonably well using m = 1.50 - 0.65i. In addition, the measured optical density ratios lie about 25% below the theoretical curve for both room temperature and high temperature tests. Furthermore, it was impossible to fit the OD_R/OD_B and $I_{\parallel}/I_{\perp}$ data simultaneously using any other reasonable values of n and k or by assuming reasonable variations of n and k with wavelength. A possible source of the discrepancies in these data is the nonspherical shape of the soot particles, which are known to consist of large irregular or chainlike agglomerates of smaller nearly spherical soot particles.

Volume fractions for flaming combustion of the polyphosphazene insulation material were calculated using m = 1.57 - 0.56i as the refractive index for soot. These curves are presented in Fig. 22 and are corrected to the standard volumetric flow rate of 142 l/min to eliminate the dilution effect at high temperatures. The peak volume fractions are also given in Table 4; these values exhibit the same trend with increasing ambient temperature as the optical density. Again smoke concentration appears to be the primary factor influencing the light-obscuring properties of the smoke produced by flaming combustion of this material.

Values of the total particulate volume were obtained by integrating the volume fraction curves in Figs. 19 and 22 with respect to time. These values were then normalized by dividing by the unburned sample weight to yield a specific total particulate volume (i.e., total particulate volume per unit mass of material burned). Values of the specific total particulate volume (STPV) for both flaming and nonflaming modes are also given in Table 4. For nonflaming combustion, the STPV, like the peak volume

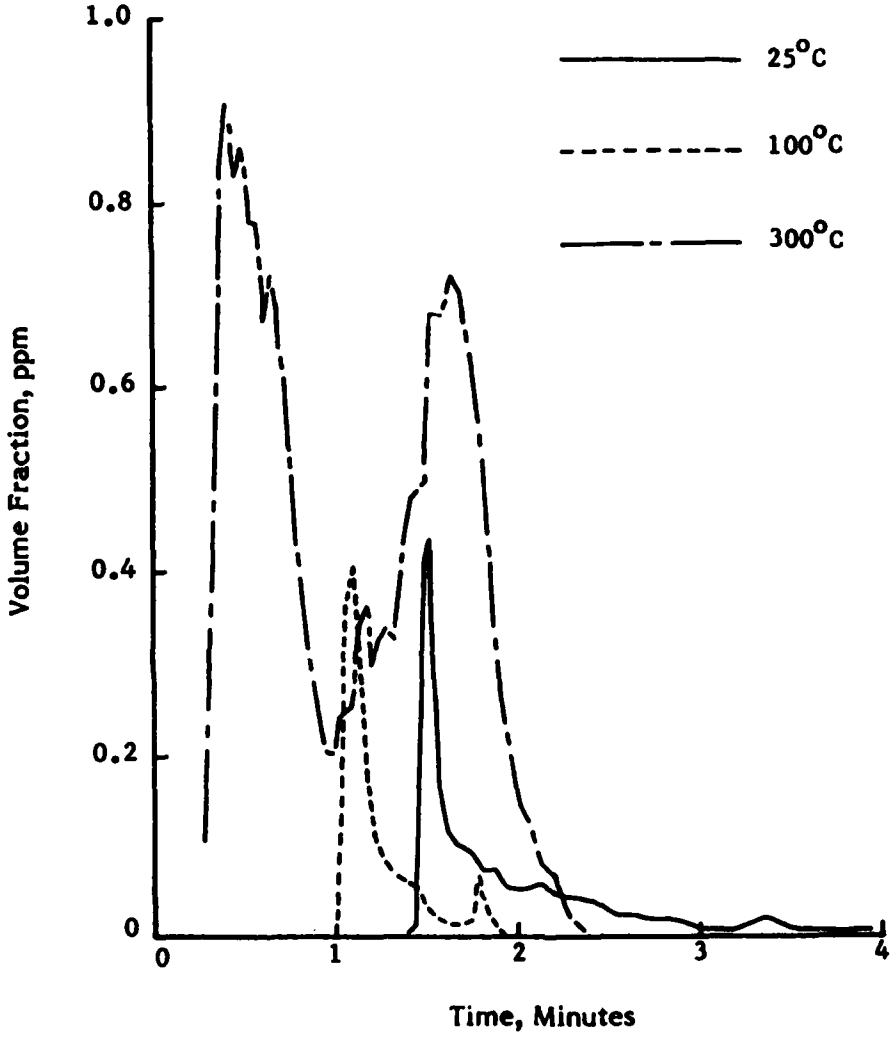

Figure 22. Effect of the ventilation air temperature on the particulate volume fraction for flaming combustion of polyphosphazene insulation material exposed to a radiant flux of 5 W/cm^2.

fraction, decreases rapidly as the ambient temperature is increased, becoming essentially zero at 300°C. Furthermore, increasing the radiant flux from 5 W/cm^2 to 7.5 W/cm^2 in the room temperature environment nearly doubles the total volume of smoke particulates produced. In contrast, the STPV for flaming combustion at 300°C is over five times greater than the corresponding value at 25°C, and it is least for 100°C. This latter result is due to the much longer period of strong flaming combustion which occurs at 300°C, in contrast to the very brief period of strong flaming followed by weak intermittent flaming which occurs at the lower temperatures. This result is also evident by comparing the areas under the volume fraction versus time curves for flaming combustion given in Fig. 22.

Although no sampling data were available for elevated temperatures, the effect of ambient temperature on Γ was estimated from the optical data. These data are also given in Table 4 for both flaming and nonflaming combustion, were Γ is normalized with respect to the corresponding room-temperature value. The Γ values for both modes of combustion follow the same trends with increasing ventilation air temperature as the specific total particulate volume.

With the assumption of a particulate density ρ_p = 1.3 g/cm^3 for smoke particles produced by nonflaming combustion and ρ_p = 2.0 g/cm^3 for soot produced by flaming combustion, the total particulate mass was estimated from the optically determined total particulate volume. For the room temperature tests, the optically determined values of the total particulate mass were then compared with the corresponding values estimated by particulate sampling. For nonflaming combustion with the 7.5 W/cm^2 radiant flux and for flaming combustion, the agreement was quite good; here the optically determined particulate masses were about 35% greater than those obtained by sampling. These differences are easily accounted for by losses in the sampling system and uncertainties in the particle density. For nonflaming combustion at 5 W/cm^2 the agreement was not as good; here the optically determined particulate masses were about

2 ½ times greater than the particulate masses obtained by sampling. In this case, however, the optical density values upon which the optical particulate masses are based were less accurate due to the low concentration of smoke produced during these tests.

Values of the specific total particulate volume (STPV) given in Table 4 can be used to estimate the smoke volume concentration and optical density for the polyphosphazene insulation material burning in a confined space. The STPV value is first multiplied by the total mass of polymer originally present in the compartment to obtain the total volume of the smoke particulates produced during combustion. Assuming that all of the smoke is uniformly distributed throughout the compartment, the volume fraction φ is next obtained by dividing the previous result by the compartment volume. To obtain the optical density Eqs. (A-3) and (A-5) are combined to yield:

$$OD_B = 0.651 \quad \bar{Q}_{ext}(D_{32}, m_B)\ \varphi/D_{32}$$

where D_{32} is obtained from Table 3, m_B is obtained from Table 4, and $\bar{Q}_{ext}$ is calculated from Eq. (A-6) using the Mie scattering theory. As an example, consider a 10 ft x 10 ft bulkhead covered with ½-inch thick polyphosphazene insulation burning in a 25,000 ft^3 (708 m^3) space. The weight of the unburned polymer in this case is 16.72 kg. From Table 4 the worst nonflaming case occurs for a 7.5 W/cm^2 radiant flux in room temperature air, for which the STPV is about 0.024 cm^3/g, while only slightly more particulates are produced for the worst flaming case which occurs in 300°C air. The worst case values of volume fraction are 0.57 ppm for nonflaming combustion and 0.62 ppm for flaming combustion, while the corresponding values of optical density (blue) are 2.2 m^{-1} and 0.85 m^{-1} respectively. From this example, it is clear that greater light obscuration occurs under nonflaming conditions at high heating rates than for flaming combustion. For the nonflaming case the light attenuation is rather severe, amounting to less than 1% of the incident

light transmitted over a one meter optical path length. It is unlikely that such large amounts of the polyphosphazene insulation material will undergo nonflaming combustion in an actual fire, however, since the radiant flux would have to be supplied by flaming combustion of neighboring materials. Thus flaming combustion of the polyphosphazene material would be expected to occur, especially if the ambient temperature rises above 300°C. In this case the light obscuration is much less severe, amounting to a 14% transmission of blue light over a one meter optical path length.

These are the changes for the chemistry part from Dr. Brenner.

CHEMICAL ANALYSIS OF SMOKE PARTICULATES

The work carried out during the current grant period has been in two major areas, namely investigation of smoke produced from combustion of polyphosphazene insulation material, and fundamental studies aimed at improving understanding of the chemistry of smoke formation.

Polyphosphazene Combustion Products

The composition of the polyphosphazene material supplied by the ~~Office of~~ Naval Research Laboratory was not precisely known. The manufacturing source (Horizons Co.) is no longer in operation, and personnel originally responsible for its production were unable to supply detailed information on the polymer. However, the description which follows is believed to be generally correct, although lacking detail.

The polymer is based on the 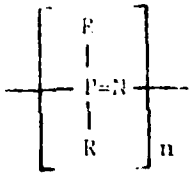 unit backbone. The functional group R may be either 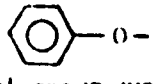 or 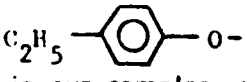 . It was not known which functional group was present in our samples, or whether this would make any significant difference to the test results. Additives present in the formulation were alumina trihydrate ($Al_2O_3 \cdot 3H_2O$), magnesium oxide (MgO), benzoyl peroxide ($(C_6H_5 \cdot CO_2)_2$) and dialkyl phthalate ($C_6H_5(COOR)_2$).

Experimental Procedure. The polyphosphazene samples were subjected to $5 W/cm^2$ incident heat flux for nonflaming oxidative pyrolysis. Flaming studies were not carried out, as it proved impossible to sustain a flaming mode of combustion for sufficient time to collect smoke particles reliably. All data, therefore, refer to nonflaming combustion studies. Smoke samples were obtained using the CPTC, with collection on a dual Gelman glass fiber filter trap. Smoke samples were obtained with a probe located at

approximately the same height as that used for optical scattering measurements.

Chemical analysis was performed using established analytical procedures developed in this laboratory [9,10]. Instrumentation used included a Hewlett-Packard model 5710A gas chromatograph with flame ionization detector, a Hewlett-Packard model 5720A gas chromatograph with thermal conductivity detector, and a Hewlett-Packard model 5700A/5982A gas chromatograph/mass spectrometer system with a combined electron impact/chemical ionization source and a model Hewlett-Packard 2100S microprogrammable systems computer for data collection and peak identification.

Results and Discussion. The mass of smoke produced in the nonflaming mode was relatively low, comprising only 8.5 mg smoke particulates per gram of polyphosphazene insulation pyrolyzed. Of this particulate smoke, approximately 27% by weight was in the form of organic compounds which could be extracted into methylene chloride solvent, using a Sohxlet extraction procedure. These results are summarized in Table 5.

Extensive analysis by gc/ms of the extractable components of the smoke indicated that the majority of the smoke consisted of aliphatic hydrocarbons (63.7%) and oxygenated aliphatic hydrocarbons (19.4%) (Table 6). Smaller amounts of aliphatic nitrile, polynuclear aromatic and oxygenated aromatic compounds were also found. These compounds are all liquid at low temperatures (25-200^{o}C) with refractive indices between 1.42 and 1.46, in good agreement with values obtained with the in situ optical system (Table 4). It is interesting to note that no phosphorus-containing compounds were detected in the particulate smoke, in spite of extensive searches of the mass spectral data in an attempt to identify organophosphorus species. It is likely, although detailed analysis was not carried out to confirm this, that the majority of the phosphorus present in the polymer remains as inorganic phosphates or phosphorus oxy-compounds

Table 5. Combustion Products from Non-Flaming Tests of Polyphosphazene

	Yield (mg/g of Polyphosphazene)
Smoke Particulate	8.5
Extractable Organic Compounds (EOC)	2.3
% EOC/Smoke	27.1

Table 6. Classes of Products Found in Smoke Particulates

	Aliphatic Hydrocarbons	Oxygenated Aliphatic Hydrocarbons	Aliphatic Nitriles	Polynuclear Aromatics	Oxygenated Aromatics
	$C_{12}H_{24}$	$C_9H_{17}CO_2H$	$C_{15}H_{31}CN$	Pyrene	Phthalate ester
	$C_{13}H_{28}$	$C_{11}H_{20}O$	$C_{16}H_{33}CN$	Benzofluorene	Benzoate ester
	$C_{18}H_{38}$	$C_{18}H_{36}O$	$C_{17}H_{35}CN$	Chrysene	___
Amount by Weight	63.7%	19.4%	5.1%	2.5%	9.3%

in the char. In terms of toxic hazard, the most toxic compounds present are those containing the aliphatic nitrile (CN) group, such as pentadecylnitrile, $C_{15}H_{31}CN$, hexadecylnitrile, $C_{16}H_{33}CN$ and heptadecylnitrile, $C_{17}H_{35}CN$. These compounds themselves exhibit some toxicity, although probably considerably less than lower members of the series, such as propionitrile, C_3H_7CN, which resemble cyanides in their toxicity. Precise measures of aliphatic nitrile toxicity are currently unavailable. At high temperatures, however, as might be present in an actual fire, aliphatic nitriles thermally decompose to release hydrogen cyanide. The toxicity of this compound is well characterized, with a threshold limit value (TLV) of 11 mg/m^3. If complete decomposition of the released aliphatic nitriles is assumed, then the anticipated concentration of HCN produced from a 10 ft by 10 ft bulkhead burning into a 25,000 ft^3 space would be approximately 12.7 mg/m^3. This cyanide level would be well below the level likely to cause acute toxic hazard to personnel exposed to the gases in a fire.

(with polyphosphagenes) An additional point of direct relevance to soot formation is the influence of inorganic additives on the combustion products of plastics. Based on studies with various PVC formulations, we conclude that certain inorganic additives, namely lead sulfate $Pb_2(SO_4)_3$ stabilizer and alumina trihydrate $Al_2O_3 \cdot 3H_2O$ fire retardant may only affect the physical steps in the polymer soot formation processes. It appears that anti-soot effects of $Al_2O_3 \cdot 3H_2O$ may result from the endothermic dehydration of this metal oxide at high temperatures[20,21] 11,12. This, in turn, may reduce the rate of fuel production from the solid polymer through the thermal degradation process.

On the other hand, the lead sulfate salt may suppress soot production by interference of the Pb^{+3} ion in the agglomeration processes through electrical charging of soot precursors[22,3].

SUMMARY AND CONCLUSIONS

~~Under Task A of this program~~, smoke physical properties were determined for a polyphosphazene foam, which is being considered by the Navy for use as a thermal and acoustic insulation material in submarines. These properties were determined for both smoldering and flaming combustion in both room-temperature and high-temperature atmospheres. The results of these tests are summarized below:

(1) For nonflaming combustion at higher heating rates (7.5 W/cm^2) in room temperature air, the polyphosphazene foam produces smoke consisting of spherical yellowish liquid droplets along with particles of a darker, brown, possibly solid material. The particle size distribution is log-normal with a mass median diameter (D_{MMD}) of about 0.5 micron and a geometric standard deviation (σ_g) of about 1.4. At lower heating rates (5 W/cm^2) the darker material is absent, but the amount of smoke produced is insufficient to obtain a particle size distribution. The mean particle diameter D_{32} obtained with the in situ optical system for both heating rates is about 0.45 micron, which is in good agreement with D_{MMD} obtained by cascade impactor sampling. The particle refractive index at peak optical density ranges from 1.35 at 5 W/cm^2 to 1.45 at 7.5 W/cm^2.

(2) At low environmental temperatures, strong flaming combustion was brief followed by weak, intermittent flaming. During flaming combustion the polyphosphazene produced black smoke consisting of nonspherical soot aggregates with a mean particle diameter (D_{32}) between 0.9 and 1.2 microns and a refractive index of about 1.57-0.56i.

(3) In room temperature air under 5 W/cm^2 radiant flux, the polyphosphazene foam converts about 2% of its total mass loss into smoke particulates for both flaming and nonflaming combustion.

Under smoldering combustion at 7.5 W/cm^2 this material yields about 5% of its total mass loss as particulates.

(4) For a sample mass of about 10g with ventilation air flow rates of about 140 liters/minute, the polyphosphazene foam produced the greatest light obscuration under nonflaming combustion at the higher heating rate (7.5 W/cm^2), which gave an optical density in blue light of about 1.2 m^{-1}. For nonflaming combustion at 5 W/cm^2, however, light obscuration was slight, amounting to only 0.2 m^{-1}. Under flaming combustion, optical density reaches a brief peak of about 0.6 m^{-1}, but drops rapidly to below 0.1 m^{-1}.

(5) For nonflaming combustion of the polyphosphazene foam, moderate increases in ambient temperature result in decreases in peak volume fraction and total particle volume, while the peak optical density and the mean particle diameter remain about the same. In higher temperature environments (about 300°C and above), the polyphosphazene foam produces little or no particulates and the peak optical density of about 0.6 m^{-1} results from absorption by gaseous pyrolysis products. These results are consistent with a condensation mechanism for smoke production.

(6) For flaming combustion of the polyphosphazene foam, moderate increases in ambient temperature have little effect on peak optical density and peak volume fraction, while total particulate volume is decreased. There is a definite trend of increasing mean particle diameter with increasing environmental temperature. In atmospheres at 300°C and above, the period of strong flaming combustion is much longer than at the lower temperatures resulting in much larger values of peak optical density, peak volume fraction, and especially total particle volume.

The smoke properties of the polyphosphazene foams may also be compared with the PVC-nitrile rubber wall insulation material tested previously[6]. Under nonflaming conditions the smoking tendency I of the polyphosphazene foam is about a third of that obtained previously for the PVC-nitrile rubber, while both materials have about the same value of I under flaming combustion. The polyphosphazene foam produces smaller particles during nonflaming combustion and slightly larger particles during flaming combustion than the PVC-nitrile rubber. The optical density, peak volume fraction, and specific total particulate volume (STPV) obtained during room temperature tests of the polyphosphazene material for both flaming and nonflaming combustion are all much less than the corresponding quantities for similar tests of the PVC-nitrile rubber material. In particular, the STPV values for the polyphosphazene foam are only about a fifth for nonflaming combustion and a tenth for flaming combustion of the corresponding STPV values obtained for the PVC-nitrile rubber. These results indicate that the loss of visibility due to smoke formation during combustion of the polyphosphazene foam in shipboard fires is considerably less than that obtained with the PVC-nitrile rubber insulation.

The chemical analysis of the smoke particulates generated during nonflaming combustion of the polyphosphazene foam indicated the presence of aliphatic hydrocarbons, oxygenated aliphatic hydrocarbons, aliphatic nitriles, polynuclear aromatic hydrocarbons (PAH) and oxygenated aromatic compounds, while organophosphorous compounds were not detected. The level of hydrogen cyanide expected from thermal decomposition of the aliphatic nitrile species in the smoke is well below the amount likely to produce acute toxic hazard to personnel exposed to gases in a fire.

APPENDIX A

PHYSICAL PROPERTIES CHARACTERIZING SMOKE

This appendix gives a brief discussion of each of the smoke physical properties which were measured during this research program.

Particle Size Distribution. Particle size distributions are presented as cumulative type curves which are generated by plotting the percentage of particulate weight having particle diameters less than a given particle size versus the particle size on log-normal probability type paper[23,14]. These data are taken from Andersen Sampler (cascade impactor) measurements, and when the weight distribution of the particle sizes is log-normally distributed, the curves appear as straight lines[23,14]. Also, note when the mass-size distribution is log-normally distributed the number and surface-size distributions are also log-normally distributed with the same standard deviation[23,14]. In the presentation of this data, the cumulative size distribution plots have been represented when practicable by a straight line corresponding to a log-normal distribution. The mass median diameter (D_{MMD}) is readily obtained from these cumulative probability plots; fifty percent of the sampled particulates (by mass) are composed of particles of diameters less (or greater) than the mass median diameter[23,14]. The geometric standard deviation (σ_g) is also calculated from the log-normal plots according to the following formula given by Cadle[23,14]:

$$\sigma_g = \frac{D(84.13\%)}{D_{MMD}} = \frac{D_{MMD}}{D(15.87\%)} \qquad \text{(A-1)}$$

The geometric standard deviation is an indication of the relative spread of particle diameters about the mean diameter where about 68% of the particles have diameters between D_{MMD}/σ_g and $\sigma_g D_{MMD}$. Although the data shown does not always follow a log-normal distribution, the authors believe that the values of σ_g calculated from the cumulative probability plots gives a general indication of the dispersity of the data thus providing a

reasonable basis for comparisons.

Mass Fraction of Fuel Converted to Particulates. The weight of the collected particulates is used to calculate the fraction of the sample weight loss which becomes particulate matter (Γ). This provides an indication of the tendency of a material to generate smoke per unit mass of fuel expended.

Mean Particle Diameter. The forward scattering light intensity measurements obtained with the In Situ Optical Aerosol Measurement System were used to determine the volume-surface mean particle diameter (D_{32}) as a function of time during each test. The volume-surface mean diameter is defined as follows:

$$D_{32} = \frac{\int_0^{D_\infty} N(D)D^3 dD}{\int_0^{D_\infty} N(D)D^2 dD} \qquad \text{(A-2)}$$

where N(D) is the number size distribution, D is the particle diameter, and D_∞ is the maximum particle diameter. Using blue-green light from an argon-ion laser (λ = 488 nm), measurements were made of the ratio of scattered light intensities at two forward angles (5^o and 15^o) from which D_{32} was determined by diffractive scattering theory[15,24]. The measurement of D_{32} by this forward scattering ratio technique is relatively insensitive to the particle refractive index and concentration (unknown), and the shape of the size distribution function. In calculating D_{32} from the measured intensity ratio, the "Upper Limit Distribution Function" used by Mugele and Evans[16,25] and later by Dobbins and Jizmagian[17,26] was assumed. In addition to the plots of D_{32} versus time, the value of D_{32} corresponding to maximum light obscuration (i.e., peak optical density) was determined for each test.

Optical Density. The transmitted blue-green light from the argon-ion laser and the transmitted red light from a He-Ne laser (λ = 633 nm) were used to determine the optical densities at these two wavelengths as a function of time. The smoke optical density per unit optical path length is defined as follows:

$$OD = \frac{\log_{10} \frac{I_o}{I}}{L} \qquad (A-3)$$

where I_o is the incident light intensity, I is the light intensity transmitted through the smoke, and L is the optical path length (0.114 meter for the CPTC). This data is presented as plots of the optical density in blue-green light (OD_B) versus time. In addition maximum optical densities (OD_{max}) at both wavelengths were determined for each test. The increased dilution of the smoke by the higher volumetric flow rate of the hot ventilation air in the high temperature tests tends to reduce the optical density of the smoke. In order to eliminate this dilution effect, the high temperature OD_{max} data has been corrected to the same volumetric flow rate as the 25°C data using the following formula:

$$OD_{corr} = OD_{meas} \left(\frac{\dot{V}_t}{\dot{V}_{25}} \right) = OD_{meas} \left(\frac{T + 273}{298} \right) \qquad (A-4)$$

where $\dot{V}_T$ and $\dot{V}_{25}$ are the volumetric flow rates at high temperature and at 25°C respectively and T is the ventilation gas temperature in degrees Celsius.

Particle Refractive Index. In order to obtain the volume concentration of the smoke particles from the measured optical densities and mean particle diameters, it is necessary to know the refractive index ($m = n - ik$) of the smoke particles. It has been shown in Reference 3 for nonabsorbing, spherical particles of known D_{32} that the real part of the refractive index n (the imaginary part is zero) can be determined from the

ratio of optical densities at two widely separated wavelengths provided the refractive index is independent of wavelength. Thus measurements of the ratio of optical density in red light (λ = 633 nm) to the optical density in blue light (λ = 488 nm) were made for each of the ~~materials studied in Task A.~~ test conditions. This optical density ratio (OD_R/OD_B) along with the measured values of D_{32} was used to calculate values of n for the nonflaming tests since smoke particulates produced under nonflaming conditions usually consist of tarry liquid droplets which are assumed to be nonabsorbing; that is, the imaginary part (absorption index, k) of the refractive index is either zero or very small.

The above method of determining the refractive index of smoke particles fails if the smoke particles have significant values of the absorption index, k. In order to determine both n and k additional information is needed. Thus, two additional detectors have been incorporated into the optical system to measure blue-green light (λ = 488 nm) scattered in the plane perpendicular to the incident light beam. These detectors measure the 90° - scattering intensities parallel to ($I_\parallel$) and perpendicular to ($I_\perp$) the plane of polarization of the incident light beam. Using the Mie scattering theory[27, 16], the ratio of $I_\parallel/I_\perp$ can be used along with the mean particle size D_{32} (from the forward scattering measurements) and the ratio of optical densities at the two laser wavelengths to obtain the complex refractive index, m, of the smoke particles. In practice the values of n and k can be determined from measurements of D_{32}, OD_R/OD_B, and $I_{11}/I_\perp$ only if (1) the absorption index k is not too large ($k < 0.4$), (2) n and k are both independent of wavelengths for the wavelengths used, and (3) the smoke particles are spherical and homogeneous.

Values of $I_\parallel/I_\perp$ were measured for most of the tests conducted ~~under Task A.~~ For polyphosphazene. For the nonflaming tests, the measured values of $I_\parallel/I_\perp$ and D_{32} were used to calculate the refractive index n under the assumption of (1) k = 0 and (2) wavelength independence of n for the smoke produced in smoldering combustion. For flaming combustion, the particulates consist of

highly absorbing carbonaceous material (soot) with a refractive index of approximately $m = 1.57 - 0.56i$[8]. Thus the values of $I_{\parallel}/I_{\perp}$ and OD_R/OD_B measured in the flaming tests are compared with the values computed using the Mie theory with $m = 1.57 - 0.56i$.

Particulate Volume Fraction. The concentration of the smoke particles is determined from the optical density in terms of the particulate volume fraction or volume concentration, which is the volume of particles contained in a unit volume of gas-particle mixture (i.e., aerosol). Using the previously determined mean particle diameters (D_{32}) and refractive index (m), the volume fraction (φ) was calculated from the blue-green light transmission measurements using the following expression:[3,26,17]

$$\varphi = \frac{2}{3}\left(\frac{D_{32}}{\bar{Q}_{ext}(D_{32},m)\ L}\right)\ln(I_o/I)_B \qquad \text{(A-5)}$$

where $\bar{Q}_{ext}$ is the mean extinction efficiency given by[26]

$$\bar{Q}_{ext} = \frac{\int_o^{D_\infty} Q_{ext}(D,m)\ N(D)\ D^2 dD}{\int_o^{D_\infty} N(D)\ D^2\ dD} \qquad \text{(A-6)}$$

Thus plots of volume fraction φ versus time were obtained for each of the tests conducted on Polyphosphazene in Task A. In these plots the volume fractions for the high temperature tests have been corrected to the standard flow rate of 142 l/min according to the formula:

$$\varphi_{corr} = \varphi_{meas}\left(\frac{\dot{V}_T}{\dot{V}_{25}}\right) = \varphi_{meas}\left(\frac{T+273}{298}\right) \qquad \text{(A-7)}$$

The total volume of smoke particulates produced during each test was then estimated by integrating the φ versus time curve and multiplying by the constant volumetric flow rate for the test, thus

$$V_p = \dot{V}_T \int_o^{t_{max}} \varphi \, dt \qquad \text{(A-8)}$$

If the density of the particulates (ρ_p) is known, the total particulate mass is then given by:

$$m_p = \rho_p V_p \qquad \text{(A-9)}$$

and the fraction of sample weight loss converted to particulates (Γ) is given by:

$$\Gamma = \frac{m_p}{M_i - M_f} \qquad \text{(A-10)}$$

where M_i and M_f are the initial and final sample masses respectively. Values of Γ thus obtained optically were then compared with the Γ values obtained from the collected samples for the low temperature tests.

Sample Weight Loss. For each test the weight of the burning sample was monitored continuously, and the results are plotted as curves of percent initial weight versus time. From the maximum slope of the weight loss cuve the peak mass loss rate per unit sample area was also obtained. Finally the amount of char residue, if any, was determined as a percentage of the initial sample weight.

APPENDIX B
REFRACTIVE INDICES AND BOILING POINTS OF ORGANIC LIQUIDS

In order to interpret the refractive index data for smoke particulates obtained during nonflaming combustion of various materials, refractive indices are needed for organic liquids which are likely to be present in the smoke particles. Since these smoke particles are usually produced by condensation of pyrolysis vapors upon mixing with the cooler ventilation air, data on the boiling points of these compounds are also desired. Therefore a list of 82 organic compounds, most of which have melting points below 20°C and boiling points between 20°C and 350°C, has been compiled from Reference ~~28~~ 19. This data is given in Table B-1, where chemical formula, molecular weight, boiling point at 1 atm pressure, and refractive index at 20°C for the wavelength of the sodium D line (589 nm) are given for each compound. The compounds are listed in order of increasing boiling point. Most of the compounds in Table B-1 were selected on the basis of previous data on the classes of compounds present in the smoke produced during nonflaming combustion or oxidative pyrolysis, while others were included for comparison purposes. These include aliphatic hydrocarbons (alkanes, alkenes, and alkynes), alcohols, aldehydes, ketones, ethers, carboxylic acids, aromatic hydrocarbons, polycyclic aromatic hydrocarbons (PAH), amines, nitriles, and chlorinated hydrocarbons. The data given in Table B-1 are also plotted as refractive index versus boiling point in Fig. B-1, where the compounds are identified by the numbers used in Table B-1.

Examination of Fig. B-1 and Table B-1 reveal a number of interesting facts. When all classes of organic compounds are considered, there is little correlation between refractive index and boiling point, since for a given boiling point there is a large range in possible refractive indices. On the other hand, if only a single class of compounds is considered, there is a well defined trend of increasing boiling point and refractive index as the number of carbon atoms is increased. Such curves of refractive index versus boiling points are shown in Fig. B-1 for the alkanes, alkenes, and alkynes. For these aliphatic hydrocarbons it is also seen that the refractive index increases as the number of hydrogen atoms decreases (for constant number of carbon

atoms). It is also seen that relatively few compounds lie below the alkane curve; these include methanol and ethanol, a few carboxylic acids, a few nitriles, acetaldehyde, and acetone. A few exotic fluorine containing organic compounds have unusually low refractive indices for a liquid (between 1.26 and 1.29), but these are not expected in the combustion products of typical materials. Most of the non-aromatic compounds listed in Table B-1 lie between or near the alkane and alkyne curves in Fig. B-1. Aromatic compounds, however, have considerably larger refractive indices than the aliphatics as illustrated by a number of aromatic hydrocarbons, ethers, aldehydes, ketones, nitriles, and amines as well as PAH's (naphthalene). Also chlorinated aliphatic hydrocarbons have considerably larger refractive indices than aliphatic hydrocarbons of similar boiling point. The compound in the list with the largest refractive index is carbon disulfide (n_D = 1.628), which is not expected to be present in the combustion products of typical materials.

On the basis of the data presented in Figure B-1 and Table B-1, the following can be concluded regarding the refractive indices of smoke particulates produced during nonflaming combustion of polymeric materials. The smoke particles are expected to be spherical liquid droplets consisting of a mixture of a large number of organic compounds similar to those listed in Table B-1. For materials, such as polyphosphazene, where the smoke particles consist predominately of aliphatic hydrocarbons, the refractive indices are expected to be in the range 1.35 to 1.45. For other materials which produce aromatic compounds or chlorinated compounds during pyrolysis, smoke refractive indices are expected to be considerably higher, ranging up to 1.55 or 1.6. It is also expected that for smoke particles produced in higher temperature environments, materials with higher boiling points will predominate resulting in a somewhat larger refractive index than obtained in room temperature environments.

Table B-1. Refractive Index and Boiling Points of Selected Organic Liquids.

No.	Compound	Formula	Mol.Wt.	Boiling Pt. (°C)	Refractive Index at 20°
1	Acetaldehyde	CH_3CHO	44.05	20.8	1.332
2	1-Pentene	$CH_3CH_2CH_2CH = CH_2$	70.14	30	1.372
3	Ethyl Ether	$C_2H_5O\ C_2H_5$	74.12	34.5	1.353
4	Pentane	$CH_3(CH_2)_3CH_3$	72.15	36.1	1.358
5	Trifluoroacetic acid anhydride	$(F_3CCO)_2O$	210.03	39	1.269[a]
6	1-Pentyne	$CH_3CH_2CH_2C \equiv CH$	68.13	40.2	1.385
7	Carbon disulfide	CS_2	76.14	46	1.628[a]
8	Propyl Amine	$CH_3CH_2CH_2NH_2$	59.11	47.8	1.387
9	Propanal	CH_3CH_2CHO	58.08	48.8	1.364
10	Acrolein	$CH_2 = CH\ CHO$	56.07	53	1.402
11	Acetone	$CH_3CO\ CH_3$	58.08	56.2	1.359
12	Diethyl Amine	$(C_2H_5)_2NH$	73.14	56.3	1.386
13	Chloroform	$CHCl_3$	119.38	62	1.444[a]
14	1-Hexene	$CH_3(CH_2)_3CH = CH_2$	84.16	63.3	1.384
15	Methanol	CH_3OH	32.04	65	1.329
16	Hexane	$CH_3(CH_2)_4CH_3$	86.18	69	1.375
17	Perfluorotriethylamine	$(C_2F_5)_3N$	371.05	70.3	1.262[a]
18	1-Hexyne	$CH_3(CH_2)_3C \equiv CH$	82.15	71.3	1.399
19	Trifluoroacetic Acid	$F_3C\ CO_2H$	114.02	72.4	1.283[a]
20	Butanal	$CH_3CH_2CH_2CHO$	72.12	75.7	1.384
21	Carbon Tetrachloride	CCl_4	153.82	77	1.459[a]
22	Acrylonitrile	$CH_2 = CH\ CN$	53.06	78	1.391
23	Ethanol	CH_3CH_2OH	46.07	78.5	1.361

Table B-1 Cont'd

No.	Compound	Formula	Mol.Wt.	Boiling Pt. (°C)	Refractive Index at 20°
24	2-Butanone	$CH_3CH_2CO\ CH_3$	72.12	79.6	1.379
25	Benzene	C_6H_6	78.12	80.1	1.501
26	Acetonitrile	CH_3CN	41.05	81.6	1.344
27	Trichloroethylene	$Cl\ CH = CCl_2$	131.29	87	1.475[a]
28	Triethylamine	$(C_2H_5)_3\ N$	101.19	89.3	1.401
29	Propyl Ether	$C_3H_7OC_3H_7$	102.18	91	1.381
30	1-Heptene	$CH_3(CH_2)_4CH = CH_2$	98.19	93.6	1.400
31	Propionitrile	CH_3CH_2CN	55.08	97.3	1.366
32	1-Propanol	$CH_3CH_2CH_2OH$	60.11	97.4	1.385
33	Heptane	$CH_3(CH_2)_5\ CH_3$	100.21	98.4	1.388
34	1-Heptyne	$CH_3(CH_2)_4\ C\equiv CH$	96.17	99.7	1.409
35	Diethyl Ketone	$C_2H_5CO\ C_2H_5$	86.14	101.7	1.392
36	Crotonaldehyde	$CH_3CH= CH\ CHO$	70.09	104.5	1.437
37	Toluene	$C_6H_5CH_3$	92.15	110.6	1.496
38	Ethylenediamine	$H_2NCH_2CH_2NH_2$	60.11	116.5	1.457[a]
39	1-Butanol	$CH_3CH_2CH_2CH_2OH$	74.12	117.2	1.399
40	Acetic Acid	CH_3CO_2H	60.05	117.9	1.372
41	Butyronitrile	$CH_3CH_2CH_2CN$	69.11	118	1.384
42	1-Octene	$CH_3(CH_2)_5\ CH = CH_2$	112.22	121.3	1.409
43	1-Octyne	$CH_3(CH_2)_5C\equiv CH$	110.20	125.2	1.416
44	Octane	$CH_3(CH_2)_6\ CH_3$	114.23	125.7	1.397
45	Ethyl Benzene	$C_6H_5CH_2CH_3$	106.17	136.2	1.496
46	1-Pentanol	$CH_3(CH_2)_4\ OH$	88.15	137.3	1.410
47	Propionic Acid	$CH_3CH_2CO_2H$	74.08	141	1.387

Table B-1. Cont'd

No.	Compound	Formula	Mol.Wt.	Boiling Pt. (°C)	Refractive Index at 20°C
48	Butyl Ether	$C_4H_9O\,C_4H_9$	130.23	142	1.399
49	o-Xylene	$1,2\text{-}(CH_3)_2C_6H_4$	106.17	144.4	1.506
50	Styrene	$C_6H_5\,CH = CH_2$	104.16	145.2	1.547
51	1-Nonene	$CH_3(CH_2)_6\,CH = CH_2$	126.24	146	1.414
52	Nonane	$CH_3(CH_2)_7\,CH_3$	128.26	150.8	1.405
53	1-Nonyne	$CH_3(CH_2)_6\,C \equiv CH$	124.23	150.8	1.422
54	Anisole	$C_6H_5\,O\,CH_3$	108.15	155	1.515[a]
55	1-Hexanol	$CH_3(CH_2)_5\,OH$	102.18	158	1.418
56	Furfural	$(OC_4H_3)\,CHO$	96.09	162	1.524[a]
57	Butyric Acid	$CH_3CH_2CH_2CO_2H$	88.12	165.5	1.398
58	1-Decene	$CH_3(CH_2)_7\,CH = CH_2$	140.27	170.5	1.422
59	1-Decyne	$CH_3(CH_2)_7\,C \equiv CH$	138.25	174	1.427
60	Decane	$CH_3(CH_2)_8\,CH_3$	142.29	174.1	1.410
61	1-Heptanol	$CH_3(CH_2)_6\,OH$	116.21	176	1.425
62	Benzaldehyde	$C_6H_5\,CHO$	106.13	178	1.546
63	Perfluorotributylamine	$(C_4F_9)_3\,N$	671.10	179	1.291[a]
64	Aniline	$C_6H_5NH_2$	93.13	184	1.583[a]
65	Valeric Acid	$CH_3(CH_2)_3\,CO_2H$	102.13	186	1.409
66	Benzonitrile	C_6H_5CN	103.13	190.7	1.529
67	1-Octanol	$CH_3(CH_2)_7\,OH$	130.23	194.4	1.430
68	Acetophenone	$C_6H_5\,CO\,CH_3$	120.16	202.6	1.532[a]
69	1-Dodecene	$CH_3(CH_2)_9\,CH = CH_2$	168.33	213.4	1.430
70	1-Nonanol	$CH_3(CH_2)_8\,OH$	144.26	213.5	1.433

Table B-1. Cont'd

No.	Compound	Formula	Mol.Wt.	Boiling Pt. (°C)	Refractive Index at 20°C
71	1-Dodecyne	$CH_3(CH_2)_9\ C \equiv CH$	166.31	215	1.434
72	Dodecane	$CH_3(CH_2)_{10}\ CH_3$	170.34	216.3	1.422
73	Napthalene	$C_{10}H_8$	128.19	218	1.590[b]
74	1-Decanol	$CH_3(CH_2)_9\ OH$	158.29	229	1.437
75	1-Undecanol	$CH_3(CH_2)_{11}\ OH$	172.31	243	1.439
76	Phenyl Ether	$(C_6H_5)_2\ O$	170.21	257.9	1.579[a]
77	1-Pentadecyne	$CH_3(CH_2)_{12}\ C \equiv CH$	208.39	268	1.442
78	1-Pentadecene	$CH_3(CH_2)_{12}\ CH = CH_2$	210.41	268.2	1.439
79	Pentadecane	$CH_3(CH_2)_{13}\ CH_3$	212.42	270.6	1.432
80	Benzyl Ether	$(C_6H_5\ CH_2)_2\ O$	198.27	298	1.517
81	1-Octadecene	$CH_3(CH_2)_{15}\ CH = CH_2$	252.49	312	1.445
82	Eicosane	$CH_3(CH_2)_{18}\ CH_3$	282.56	343	1.443[c]

a Refractive index at 25°C

b Refractive index at 85°C, melting point at 80.5°C

c Solid at 20°C, melting point at 36.8°C

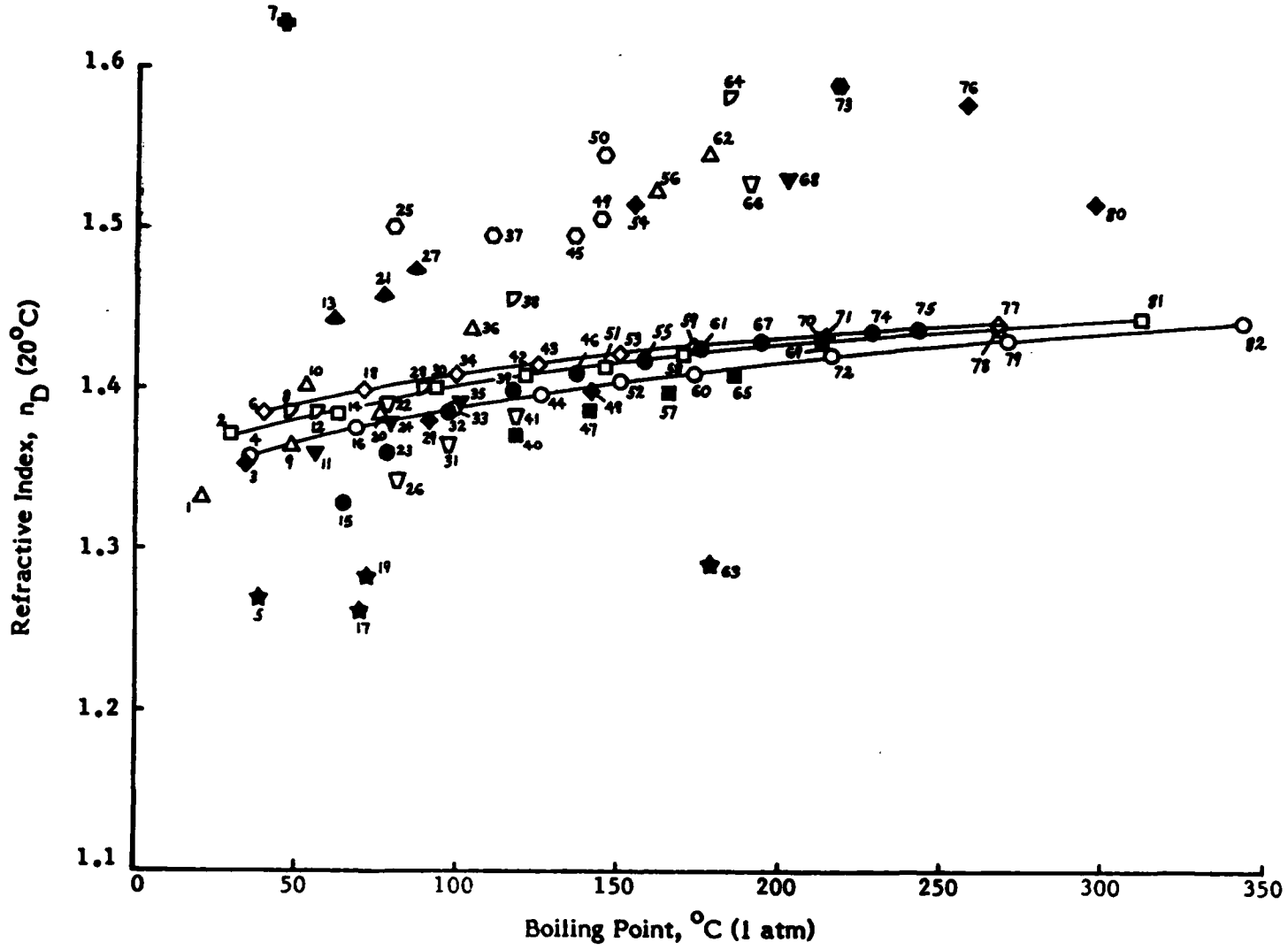

Figure B-1. Refractive index versus boiling point for selected organic liquids. Symbols: ○ alkanes, □ alkenes, ◇ alkynes, ● alcohols, △ aldehydes, ▼ ketones, ◆ ethers, ■ carboxylic acids, ○ aromatic hydrocarbons, ● PAH's, ▷ amines, ▽ nitriles, ▲ chlorinated hydrocarbons, ★ fluorine containing organics. The numbers refer to Table B-2.

REFERENCES

1. C. P. Bankston, R. A. Cassanova, E. A. Powell, and B. T. Zinn, "Initial Data on the Physical Properties of Smoke Produced by Burning Materials Under Different Conditions," J. Fire and Flammability 7, 165 (1976).

2. B. T. Zinn, E. A. Powell, R. A. Cassanova, and C. P. Bankston, "Investigation of Smoke Particulates Generated During the Thermal Degradation of Natural and Synthetic Materials," Fire Research 1, 23 (1977).

3. E. A. Powell, R. A. Cassanova, C. P. Bankston, and B. T. Zinn, "Combustion-Generated Smoke Diagnostics by Means of Optical Measurement Techniques," in Experimental Diagnostics in Gas Phase Combustion Systems (Progress in Astronautics and Aeronautics, Vol. 53), edited by Ben T. Zinn, American Institute of Aeronautics and Astronautics, New York, 1977, p. 449.

4. B. T. Zinn, R. A. Cassanova, C. P. Bankston, R. F. Browner, E. A. Powell, J. U. Rhee, and K. Kailasanath, "Investigation of the Properties of the Combustion Products Generated by Building Fires," Final Report of National Bureau of Standards grant G7-9001, Nov. 1977.

5. E. A. Powell, C. P. Bankston, R. A. Cassanova, and B. T. Zinn, "The Effect of Environmental Temperature upon the Physical Characteristics of the Smoke Produced by Burning Wood and PVC Samples," Fire and Materials 3, 15 (March 1979).

6. B. T. Zinn, R. F. Browner, E. A. Powell, M. Pasternak, and R. O. Gardner, "The Smoke Hazards Resulting from the Burning of Shipboard Materials Used by the U. S. Navy," NRL Report 8414, July 1980.

7. I. Glassman, "Phenomenological Models of Soot Processes in Combustion Systems," AFOSR TR-79-1147.

8. W. H. Dalzell, G. C. Williams and H. C. Hottel, Combustion and Flame 14, 161 (1970).

9. J. C. Liao, and R. F. Browner, "Determination of Polynuclear Aromatic Hydrocarbons in Poly-(Vinyl Chloride) Smoke Particulates by HPLC and GC/MS", Anal. Chem. 50, 1683 (1978).

10. M. Pasternak, B. T. Zinn, and R. F. Browner, "The Role of Polycyclic Aromatic Hydrocarbons (PAH) in the Formation of Smoke Particulates During the Combustion of Polymeric Materials", 18th Symposium (International) on Combustion, The Combustion Institute, pp. 91-99 (1981).

11. J. Abrahamson, "Saturated Platelets are New Intermediates in Hydrocarbon Pyrolysis and Carbon Formation", Nature 266, 323 (1977).

12. I. Glassman, "Combustion," Academic Press, New York, p. 243 (1977).

13. G. M. Badger, S. D. Jolad, and T. M. Spotswood, "The Formation of Aromatic Hydrocarbons at High Temperatures", Aust. J. Chem. 20, 1439 (1967).

14. B. T. Commins, "Atmospheric Environment", Pergamon Press, 3, 565 (1969).

15. B. D. Crittenden, and R. Long, Comb. and Flame 20, 359 (1973).

16. S. E. Stein, "On the High Temperature Chemical Equilibria of Polycyclic Aromatic Hydrocarbons", J. Phys. Chem. 82, 566 (1978).

17. K. H. Homann, and H. G. Wagner, "Chemistry of Carbon Formation in Flames", Proc. Roy. Soc. A. 307, 141 (1968).

18. J. D. Bittner, and J. B. Howard, "Composition Profiles and Reaction Mechanisms in a Near Sooting Premixed Benzene/Oxygen/Argon Flame", Eighteenth Symposium (International) on Combustion, The Combustion Institute, Pittsburgh, PA, p. 1105 (1981).

19. J. R. Sontore, and I. Glassman, "A Review of Oxidation of Aromatic Compounds", Comb. Sci. and Tech. 19, 161 (1979).

11. H. F. Mark, S. M. Atlas, S. W. Shalaby, and E. W. Pearce, Flame Retardant Polymeric Materials, edited by M. Lewin, Plenum Press, New York, p. 143 (1975).

12. C. C. Ndubizu, and B. T. Zinn, "Effects of Metallic Additives upon Soot Formation in Polymer Diffusion Flames", Comb. and Flame 46 pp. 301-314 (1982).

13. F. J. Weinberg, "Electrical Aspects of Aerosol Generation and Control", Proc. Roy. Soc. A, 307, 195 (1968).

14. R. D. Cadle, Particle Size, Reinhold, New York, 1965.

15. R. A. Dobbins, L. Crocco, and I. Glassman," Measurement of Mean Particle Sizes of Sprays from Diffractively Scattered Light," AIAA J. 1, 1882-1886, (1963).

16. R. A. Mugele and H. D. Evans, "Droplet Size Distribution in Sprays," Industrial Engineering Chemistry 43, 1317-1324 (June 1951).

17. R. A. Dobbins and G. S. Jizmagian, "Optical Scattering Cross-Sections for Polydispersions of Dielectric Spheres," J. Optical Society of America 56, 1345-1350 (Oct. 1966).

18. M. Kerker, The Scattering of Light and Other Electromagnetic Radiation, Academic Press, New York and London, 1969.

19. Handbook of Chemistry and Physics, 62nd edition, CRC Press, Boca Raton, Fla.

END

FILMED

10-84

DTIC